Master's Thesis

Numerical and Experimental Study on Micro Cross Flow Turbine Including the Prediction of Sediment Erosion

Supervisor Prof. Young-Ho LEE, Ph.D.

February 2016

Department of Mechanical Engineering
Graduate School of Korea Maritime and Ocean University

Mausam Shrestha

Table of contents

List of tables

List of figures

Numerical and Experimental Study on Micro Cross Flow Turbine including the Prediction of Sediment Erosion

Mausam Shrestha

Department of Mechanical Engineering

Graduate School of Korea Maritime and Ocean University

Abstract

A hydro plant from 5kW up to 100kW is usually responsible to provide power for a small community or rural industry in remote areas away from the grid. It gives the best solution to the power need of rural and small communities which serves as decentralized power source to meet the local population requirement. Energy requirement for lighting cooking heating drying agro processing and other small scale industries activates can be met through these Micro hydro power (MHPs) in the most reliable way in the rural areas of the country like Nepal. Cross flow turbines are widely used in such MHPs due to their simple design, easier maintenance, low initial investment and modest efficiency. Also because of their suitability under low heads, efficient operation under a wide range of flow variations and ease of fabrication.

Numerical simulation and Experimental analysis was carried out to achieve the objective of the study. Previous studies and experiment conducted in the lab were used as the reference for the further studies. Computational fluid dynamics (CFD) simulations and experiments have been conducted at various rotational speed, guide vane angle and different flow rates and the result has been compared. The previous study mostly focused on the change in the shape of the nozzle components and the casing.

Based on such design the setup has been constructed. Performance study of the setup was conducted to validate the CFD results obtained. The change in the shape of the blade has been considered in this work and the performance with the change in nozzle has been studied. CFD simulation has been conducted for the change in the shape of the blade based on the inlet angle and the diameter ratio of the turbine. The change gives positive change in the efficiency and the performance of the turbine

The structural strength of the turbine has been analyzed based on the pressure points obtained from the CFD simulations. The forces exerted by the water on the surface of the blades has been mapped on the using the Ansys Workbench Structural analysis and the stress and the deformation on the turbine blade has been studied.

Sediment erosion is one of the key challenges in hydraulic turbines especially in the Himalayan from a design and maintenance perspective in Himalayas. The effect and has been studied of sediment erosion and its effects on the turbine has been done for the various size, shape and mass flow rate of the sediment particles.

KEY WORDS: Micro-hydro Power, Hydraulic Turbine, CFD, One-way FSI, Sediment Erosion, Cross Flow Turbine

List of abbreviations

CFD	Computational fluid dynamics
CFT	Cross flow turbine
FEA	Finite element analysis
FSI	Fluid structure interaction
HPP	Hydro power plant
INPS	Integrated Nepal power system
IWM	Improved water mill
KMOU	Korea Maritime and Ocean University
kW	Kilowatt
MH	Micro hydro
MHP	Micro hydro plants
NEA	Nepal electricity authority
PV	Photovoltaic
RMS	Root mean square
RNS	Reynolds averaged Navier-Stokes
rpm	Revolution per minute
SHP	Small hydro power
SST	Shear stress transport
VFD	Variable Frequency Drive

List of symbols

α	Angle of attack	°
β	Angle between relative velocity and peripheral velocity or angle between the tangents of the blade and runner periphery	°
g	Acceleration due to gravity	m/s^2
H_e	Net head	m
η	Efficiency of turbine	%
Δp	Differential pressure between inlet and outlet	Pa
ρ	Specific water density	$kg/m3$
T	Torque	Nm
U	The peripheral velocity	m/s
V	The absolute velocity	m/s
W	The relative velocity	m/s
ω	Angular velocity	rad/s
Z	Difference in height between pressure transducer and center of the runner	m

1. Micro hydro power

1.1 Introduction

Nepal currently faces a shortage of electricity for as long as 18 hours a day in dry seasons. Owing to persistent power shortages, micro hydro power generation plays an important role in mitigating outage costs. Besides saving on energy costs, these micro hydro Power Plants ensure that industries and communities units get uninterrupted, reliable and stable supply of electricity for smooth production operations.

Nepal is land locked with limitations to energy production for electricity. But Nepal is blessed with a substantial possibility to harness water. Also, the rural communities who are deprived of a reliable source of energy can benefit from this. One of the major reasons behind this inertness is an insufficient amount of technical analysis of the turbines designed for the proposed sites. The knowledge will allow them to independently carry out design and local production of reliable small micro hydro. Out of the total potential 42,000 MW of electricity have been considered as commercially viable [1]. Currently, Nepal has been able to produce 750 MW of electricity as hydropower and connected to INPS to feed the urban areas [2].

The standalone MHP/SHP schemes cater the energy need of remote and unprivileged masses. MHP/SHPs are, therefore, proved to be instrumental to break the vicious poverty circle of the society. The number of populations benefited per kW of power of MHP is large as compared to grid connected population of urban area. Hence the social value of MHP/SHP is higher. The technology has given affordable and prompt option of MHP connection to national grid. Hence MHP/SHP will not remain as burden once the MHP area commercialize and get national grid connected. The national grid connection could not have been possible to stretch of transmission to the settlements at remote hills and mountains of the country as it is financially and technically not feasible.

Furthermore, numerous rural communities of Nepal are located in in areas which are in reach of water resources but may not be connected to national grid for some more decades to come. That may not be feasible due to both technical and financial reasons. Those areas will need MHP for moderate quantity and quality of electric thus greatly benefit from local micro hydro power installations. As such, most of the rural people in Nepal are getting electricity through renewable and alternative energy technologies such as pico hydro, micro/mini hydro, IWM and solar PV systems etc. [3].

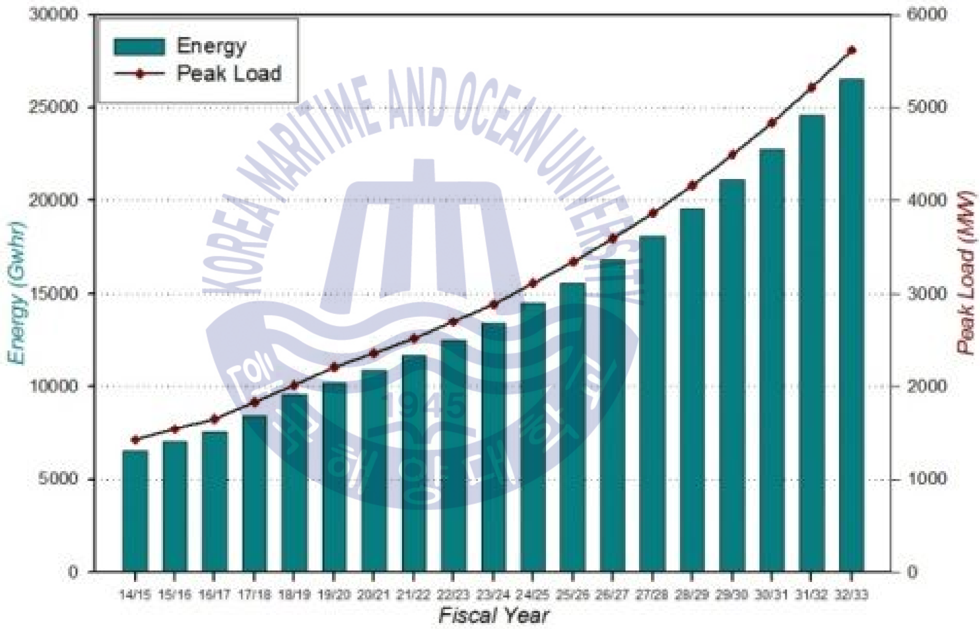

(a) Annual energy demand forecast

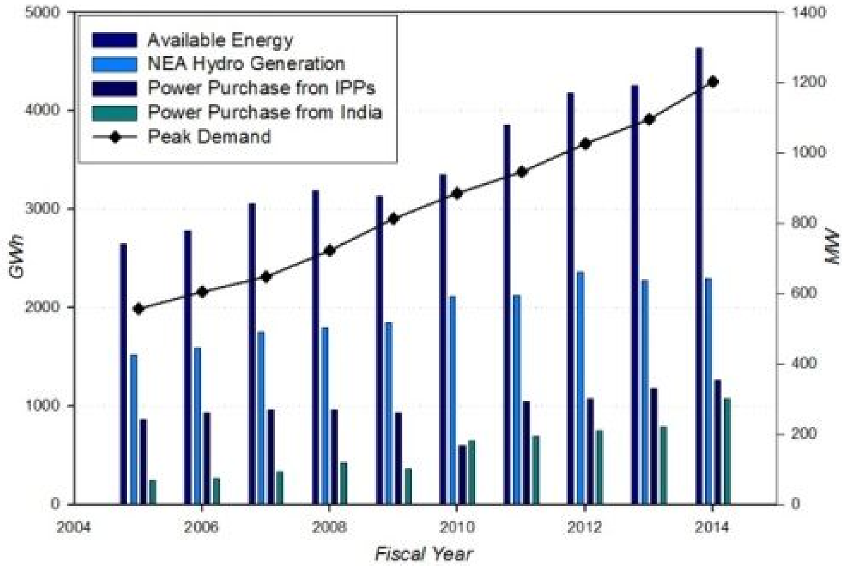

(b) Current energy production and supply

Figure 1 State of energy in Nepal [1]

Micro hydro, the technology for small sized hydropower projects of up to 100 kW, is not only to bring light into people live in the off grid locality but also give energy and water security to population, make people economically more stable, reduce the physical work load for women, enable the mechanization of rural industries and lessen environmental damages from cutting wood for fuel and heat or harming aquatic fauna and flora.

Currently, 40 MW of electricity is generating by Pico hydro (up to 10 kW), Micro hydro (greater than 10 kW but up to 100 kW) and Mini hydro (greater than 100 kW but up to 1000 kW), and providing electricity facility to 350,000 rural households [4]. Moreover, no waste or by-products are produced unlike the energy generation based on fossil sources. Many countries have begun to embrace micro hydro technology as a viable and alternative source of energy, especially for remote and rural areas. There are different replicable success stories on micro hydro based projects in many developing countries. Most of the micro hydro plants installed in Nepal have used Cross-flow turbines and Pelton turbines for power generation with more than 76% of the turbines as Cross-flow turbines [5]. Various researches have been conducted for the improvement of the performance of the cross flow turbine.

The previous research conducted in Korea Maritime and Ocean University (KMOU) has been working in the effort to improve the efficiency of the cross flow turbine. Experimental and numerical simulation has been conducted to study the performance of the turbine. Based on such result the simulation with the modification of turbine has been conducted and an improved efficiency has been obtained. Based on thus obtained efficiency, the new setup has been constructed. This research is based on the performance study of the modified setup based on the experimental and numerical analysis. In additional to it the result based on the change on the shape of the blade has been studied. One way FSI analysis for the turbine blade has been studied.

Thus Nepal needs to develop micro hydropower for the development of all sectors. The development of micro hydro can be sustainable with enhanced local capacity related to policy issues, technical issues, social issues and financial issues of micro hydro.

1.2 Research objectives

The objectives of this thesis are to

- Analyze the results of the ongoing and the past studies focused towards the modified hydraulic design of Cross flow Turbine
- Make a comparative analysis of the results between CFD and Experiment and identify the level of significance of simulation and experimental result in the field of Cross flow turbine
- Analyze the results of the ongoing studies focused for a better sediment handling

2. Hydraulic turbines

2.1 Introduction to hydraulic turbines

Hydraulic machineries are the machines that convert hydraulic power from the water to the mechanical power on the machine shaft. The purpose of a hydraulic turbine is to transform the water potential energy to mechanical rotational energy. The water energy may be either in the form of potential energy as we find in dams, reservoirs, or in the form of kinetic energy in flowing water. The shaft of the turbine directly coupled to the electric generator which converts mechanical energy in to electrical energy. Like any other machines, these machines involves various losses that arise partly in the machine itself and partly in the water transfer into and out of the machine such as pipe friction losses, losses due to bends in pipes, gates, valves and losses due to abrupt and gradual expansion and contraction of the pipes [6]. Some of the basic components of a hydropower plant are listed below

- A water diversion structure like a dam or a weir creating a gross head of water.
- A penstock, which intakes the water from the dam and transports it to the turbines. Screening is done in the intake, to prevent unwanted objects (debris and aquatic animals) entering into the turbine.
- Turbines and governing system: Electrical generators, electrical control and switching equipment, equipment housing, transformers and electricity transmission lines.
- Some of the other complementary components are the penstock gates, surge tank and a tail race if the turbine exhaust water cannot be discharged directly (through the draft tubes) into the river. Draft tubes are used to utilize the kinetic energy of the water leaving the turbine and allows the turbine to be installed above the tail water level without decreasing the available head and hence, the available power.

2.2 Types of hydro turbines

Water turbines are classified into various kinds according to i) the action of water on blades, ii) based on the direction of fluid flow through the runner and iii) the specific speed of the machine [7].

2.2.1 Classification based on the action of water on blades

These may be classified into: 1) Impulse type and 2) Reaction type

In **impulse turbine**, the pressure of the flowing fluid over the runner is constant and generally equal to an atmospheric pressure. All the available potential energy at inlet will be completely converted into kinetic energy using nozzles, which in turn utilized through a purely impulse effect to produce work. Therefore, in impulse turbine, the available energy at the inlet of a turbine is only the kinetic energy.

In **reaction turbine**, the turbine casing is filled with water and the water pressure changes during flow through the rotor in addition to kinetic energy from nozzle (fixed blades).As a whole, both the pressure energy and kinetic energy are available at the at the inlet of reaction turbines for producing power.

2.2.2 Classification based on the direction of flow of fluid through runner

Based on the flow through the turbine, the hydraulic machines are classified into:

a) Tangential or peripheral flow (Pelton)

b) Radial inward or outward flow (Francis Turbine)

c) Mixed or diagonal flow (Modern Francis turbine, Deriaz turbine**)**

d) Axial flow types (Kaplan turbine, propeller turbine)

2.2.3 Classification based on specific speed

Hydro turbines are classified on the basis of the specific speed of the turbines. The specific speed is the speed in rotations per minute at which a similar model of turbine would run under a unit head and to develop a unit power.

Table 1 Turbine classification based on specific speed

Type	Head	Specific Speed	
Low Specific Speed	200-1700m	10-30(single jet) 30-50 (Double jet)	Pelton Turbine
Medium Specific Speed	50-200m	60-400	Francis Turbine
High Specific Speed	2.5-50m	300-1000	Kaplan/ Propeller Turbine

2.2.4 Reaction turbine

In reaction turbines, only part of total head of water at inlet is converted into velocity head before it enters the runner and the remaining part of total head is converted in the runner as the water flows over it. In these machines, the water is completely filled in all the passages of runner. Thus, the pressure of water gradually changes as it passes through the runner. Hence, for this kind of machines both pressure energy and kinetic energy are available at inlet. Examples: Francis turbine, Kaplan turbines, Deriaz turbine.

Francis turbine

Francis turbine which is of mixed flow type is as shown in Figure 2. It is of inward flow type of turbine in which the water enters the runner radially at the outer periphery and leaves axially at its center [8].

The runner of turbine is consists of series of curved blades evenly arranged around the circumference in the space between the two plate. The vanes are so shaped that water enters the runner radially at outer periphery and leaves it axially at its center. The change in direction of flow from radial to axial when passes over the runner causes the appreciable change in circumferential force which in turn responsible to develop power.

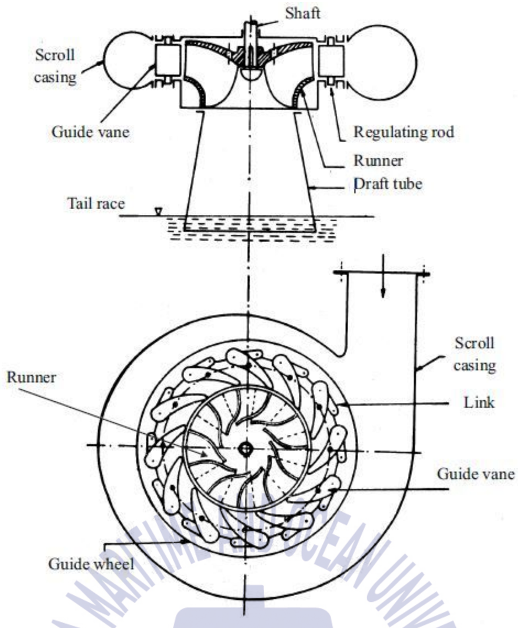

Figure 2 Sectional view of Francis turbine [8]

Propeller & Kaplan Turbines

The propeller turbine consists of an axial flow runner with 4 to 6 blades. The spiral casing and guide blades are similar to that of the Francis turbines. In the propeller turbines, the blades mounted on the runner are fixed and non-adjustable. But in Kaplan turbine the blades can be adjusted and can rotate about the pivots fixed to the boss of the runner.

The Kaplan turbine is an axial flow reaction turbine in which the flow is parallel to the axis of the shaft. This is mainly used for large quantity of water and for very low heads (4-70 m) for which the specific speed is high. The runner of the Kaplan turbine looks like a propeller of a ship. Therefore sometimes it is also called as propeller turbine. At the exit of the Kaplan turbine the draft tube is connected to discharge water to the tail race.

2.2.5 Impulse turbine

Pelton Turbine

This is an impulse type of tangential flow hydraulic turbine. It mainly possess: Nozzle and runners or buckets. Nozzle converts the potential energy into high kinetic energy. The speed of the jet issuing from the nozzle can be regulated by operating the spear head by varying the flow area. The high velocity of jet impinging over the buckets due to which the runner starts rotating because of the impulse effects and thereby hydraulic energy is converted into mechanical energy. After the runner, the water falls into tail race. Casing will provide the housing for runner and is open to atmosphere. Brake nozzles are used to bring the runner from high speed to rest condition whenever it is to be stopped. In order to achieve this water is made to flow in opposite direction through brake nozzle to that of runner.

The turgo turbine is a type of impulse turbine that is similar to the Pelton turbine but can handle higher flow rates. The incoming water jet from the nozzle strikes the plane of the runner on one side (usually at an angle of about 25°) and exits on the other side. Since the water jet interferes less with the runner than the Pelton design, it can handle more flow than a same diameter Pelton runner. Since the runner of a turgo turbine is basically a Pelton runner cut in half, a turgo turbine can generate the same power as a Pelton runner with twice the diameter and thus has twice the specific speed.

Figure 3 Different types of impulse turbines [9]

2.2.6 Cross flow turbine

Cross flow turbine is an impulse type turbine. The main characteristic of the Cross-Flow turbine it can operate from lower head till medium head. The main advantage of this turbine is that it can be operated with the similar efficiency for different flow rates. The water jet of rectangular cross-section which passes twice through the rotor blades -arranged at the periphery of the cylindrical rotor - perpendicular to the rotor shaft. It has a drum-shaped runner consisting of two parallel discs connected together near their rims by a series of curved blades.

At first, the water flow through the blade from the periphery toward the center. Then after crossing the open space inside the runner, water flows towards the runner from inside toward outside. Energy conversion takes place twice; first upon impingement of water on the blades upon entry, and then when water strikes the blades upon exit from the runner. The use of two working stages provides no particular advantage except that it is a very effective and simple means of discharging the water from the runner. A guide vane at the entrance to the turbine directs the flow to a limited portion of the runner. Thus the water strikes blades on both sides of the runner.

The machine is normally classified as an impulse turbine. Based on the fact that the original design was a true constant-pressure turbine, a sufficiently large gap was left between the nozzle and the runner, so that the jet entered the runner without any static pressure. Modern designs are usually built with a nozzle that covers a bigger arc of the runner periphery. With this measure, unit flow is increased, permitting to keep turbine size smaller. These designs work as impulse turbines only with small gate opening, when the reduced flow does not completely fill the passages between blades and the pressure inside the runner therefore is atmospheric. With increased flow completely filling the passages between the blades, there is a slight positive pressure; the turbine now works as a reaction machine.

Another feature of cross flow turbine is it always has its runner shaft horizontal (unlike Pelton and Turgo turbines which can have either horizontal or vertical shaft orientation). The cross-flow was developed to accommodate larger water flows and lower heads than the pelton.

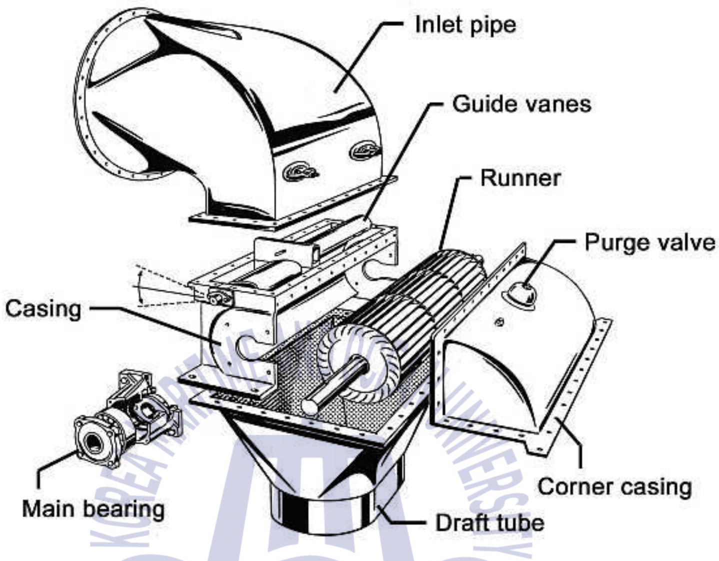

Figure 4 Cross flow turbine [10]

Cross-Flow turbines may be applied over a head range from less than 2 m to more than 100 m. A large variety of flow rates may be accommodated with a constant diameter runner, by varying the inlet and runner width. This makes it possible to reduce the need for tooling, jigs and fixtures in manufacture considerably. Ratios of rotor width/diameter, from 0.2 to 4.5 have been made. For wide rotors, supporting discs welded to the shaft at equal intervals prevent the blades from bending.

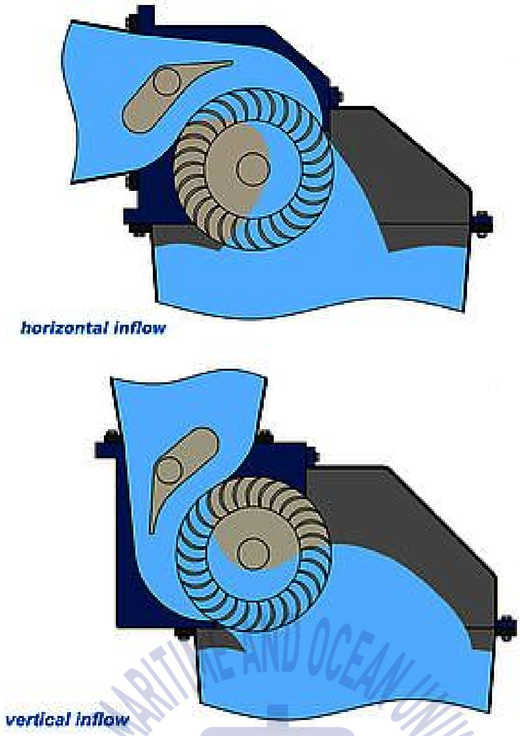

Figure 5 Horizontal flow and vertical flow cross flow turbine [10]

2.2.7 Comparison of different types of turbines

Figure 6 is a graphical presentation of a general turbine application range of conventional designs. The usual range for commercially available Cross-Flow turbines is shown in relation (dotted line). In the overall picture, it is clearly a small turbine. It shows the region of cross flow turbine among the other turbines. It benefits over other turbine over the use at low flow and low heads.

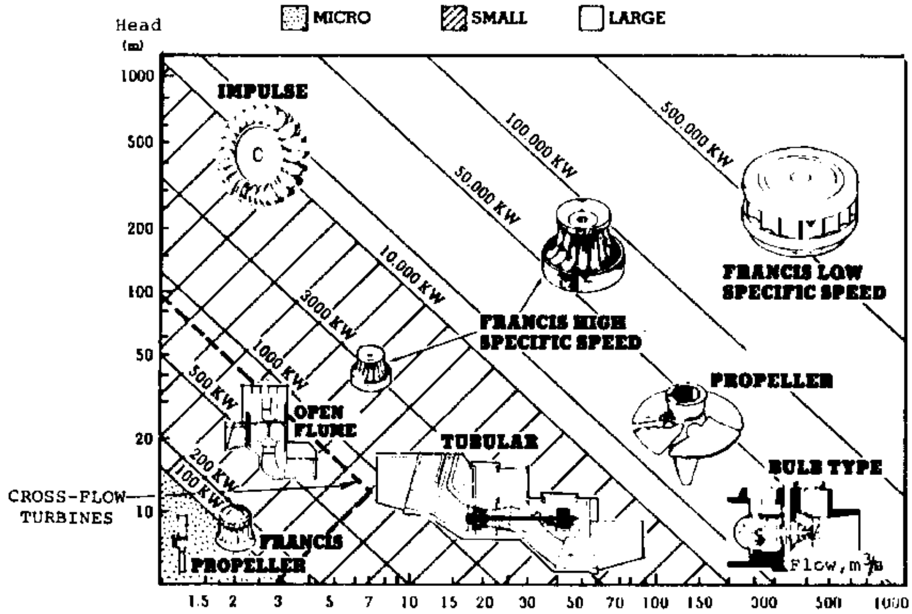

Figure 6 Application ranges of various types of hydro turbines [11]

Figure 7 shows efficiencies of some of the more important turbine types in relation to gate opening, e.g. flow rate. Conventional and highly optimized turbines achieve efficiencies of more than 90 % in large units. The Ossberger Cross-Flow has around 80 % for a wide range of flow, and the Cross-Flow turbines built in Nepal achieve over 70%. On a small unit of, say, 40 kW capacities, the maximum difference in efficiency of the Nepal Cross-Flow, and an imported conventional type would be around 10% at the optimal point. Given the same head and flow condition, this gives a reduced output for the Cross-Flow turbine of around 5 kW. Depending on turbine type, this difference is likely to be smaller or even reversed at reduced flow (e.g. Cross-Flow compared to Francis or Propeller) and also in cases where a standardized conventional turbine is installed in non-optimal conditions.

CFT is used for a wide range of heads overlapping those of Kaplan, Francis and Pelton. It can operate with discharges between 0.02 m^3/s and 10 m^3/s and heads between 1 and 200 m. Water enters the turbine, directed by one or more guide-vanes located in a transition piece upstream of the runner, and through the first stage of the runner. Flow leaving the first stage attempts to cross the open center of the turbine. As the flow enters the second stage, a compromise direction is achieved which causes significant shock losses. Around 72% of the total water energy is extracted from water in its first impact i.e. at the first stage where as remaining 28% is harvested in the second stage of the water impact. The energy of water in the form of rotational motion of the turbine is fed to the electric generator running at a specific rpm, which in turn is used for generation of electrical energy in the form of electrical current.

The utilization of these turbines in large-scale power plants has been limited due to its low efficiency compared to other turbines used commercially (η > 90%). In order to make them more competitive it is imperative that their efficiency be improved.

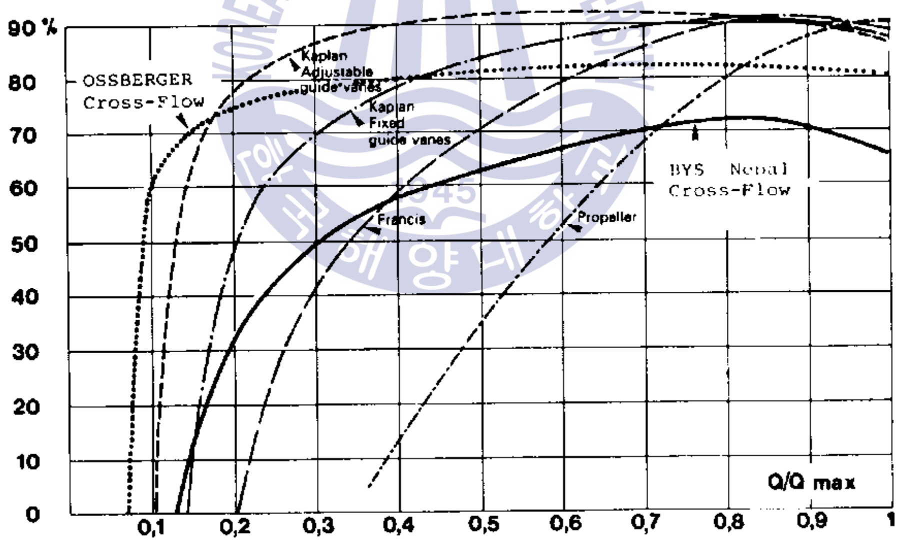

Figure 7 Efficiency curves of some turbine types [11]

2.2.8 Principle

The Cross flow turbine is a radial and partial admission free stream turbine. From its specific speed it is classified as a slow speed turbine. The guide vanes impart a rectangular cross-section to the water jet. It flows through the blade ring of the cylindrical rotor, first from the outside inward, then after passing through the inside of the rotor from the inside outward.

This flow pattern also has the advantage in practice that leaves, grass and wet snow, which when the water enters are pressed between the rotor vanes, are flushed out again by the emerging water assisted by centrifugal force - after half a revolution of the rotor. Thus the self-cleaning rotor never becomes clogged.

For the places with most prominent variation in flow rates, the cross flow (Ossberger) is built as a multi-cell turbine. The normal division in this case is 1:2. The small cell utilizes small and the big cell medium water flow. With this breakdown, any water flow from 1/6 to 1/1 admission is processed with optimum efficiency. This explains why cross flow turbines utilize greatly fluctuating water supplies with particular efficiency.

2.2.9 Efficiency

The mean overall efficiency of cross flow turbines is calculated at around 80% for small power outputs over the entire operating range. These efficiencies are normally exceeded. Efficiencies above 80% are also measured in the case of medium-sized and bigger units.

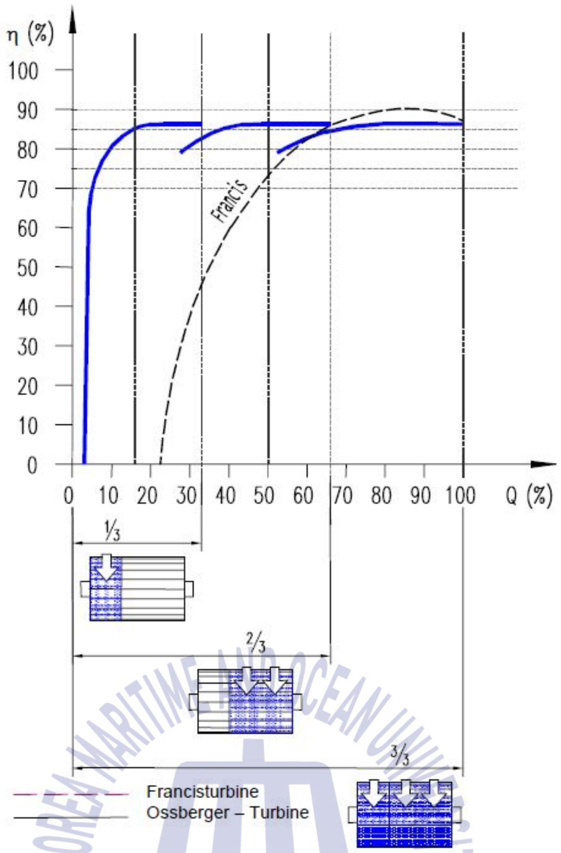

Figure 8 Efficiency characteristic of an OSSBERGER turbine developed from the 3 efficiency curves of a 1: 2 division compared with the francis turbine [10]

Figure 8 clearly illustrates the superiority of the cross flow turbine in the partial load range. Small rivers and water courses often have reduced water flow for several months of the year. Whether or not power can be generated during that time depends on the efficiency characteristics of the particular turbine. Turbines with high peak efficiency, but poor partial load behavior produce less annual power output in run-of-river power stations with a fluctuating water supply than turbines with a flat efficiency curve.

2.2.10 Casing

The casing of the turbine is entirely made of steel, exceedingly robust, lighter than a grey cast iron, impact and frost resistant.

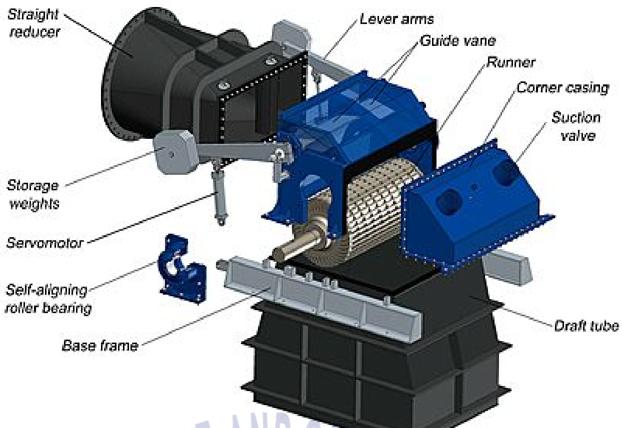

Figure 9 Design of an OSSBERGER turbine [10]

2.2.11 Guide vanes

The subdivided cross flow turbine the admission of feed water is controlled by two balanced profiled guide vanes which divide the water flow, direct it and allow it to enter the rotor smoothly independent of the opening width. Both guide vanes are fitted very precisely into the turbine casing. They keep the amount of leakage so low that in the case of small heads the guide vanes may serve as shut-off devices. Main slide valves between the pressure pipe and the turbine can then be dispensed with. Both guide vanes can be adjusted independently of one another via regulating levers to which the automatic or manual control is connected. The guide vane bearings are maintenance-free.

The nozzle of a cross flow turbine has to give a certain circumferential velocity and an optimum angle to the flow at the nozzle exit (runner inlet).

Therefore, the nozzle shape has an important influence upon the turbine performance. The influence of runner on the flow condition (flow angle and pressure distribution) is relatively small at the nozzle exit.

The nozzle exit flow has no solid boundary and the boundary condition of nozzle exit flow is the velocity on a free streamline is constant and its pressure is equal to atmospheric pressure. The two dimensional jet with free streamlines has been dealt with as a potential flow. It is common knowledge that the theoretical values about the two dimensional jet through a straight wall nozzle coincide with the experimental ones. For a curved wall jet, the exit flow has been obtained by streamline curvature method for one solid wall and by a conformal mapping and a singular curved wall.

2.2.12 Rotor

The cylindrical runner core consists of conservatively designed cam disks and, following its width, several intermediate disks to which the profiled blades are adapted and welded. This will make the runner extremely solid by stiffening it at the same time in such a way that no vibrations are faced. The blades consisting of bright drawn profiled steel mean an ideal solution regarding solidity and water guidance. By utilizing the bright-drawn and exact blade profiles an ideal balance condition is achieved automatically, only slight corrections are required on the balancing machine. The blades bent in a linear way only do not produce any axial thrust, thus there is no need for pressure bearings. Another advantage of the flow guidance is that leaves, grass or snow, pressed between the blades when the water enters the runner, are spilled out again after a half turn by the leaving water, backed-up by the centrifugal force. Thus the self-cleaning runner is never obstructed.

The rotor has up to 37 blades depending on the size. The linear curved blades produce only limited axial thrust so that the multi-collar thrust bearings with all their disadvantages are eliminated. In the case of wider rotors the blades have multiple interposed support plates. The rotors are carefully balanced prior to final assembly.

2.2.13 Flow through a cross–flow turbine

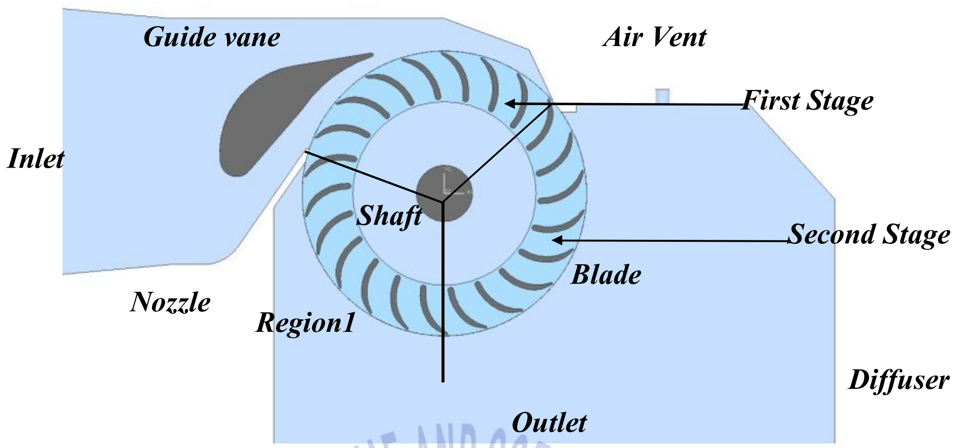

Figure 10 Cross flow operation

A cross–flow turbine in its simplest form consists of a runner and a nozzle. Figure 10 shows the manner of operation of a cross–flow turbine. The water enters through the inlet to the nozzle. The water flows through the rectangular cross–section nozzle and enters the runner through the nozzle entry arc. Nozzle entry arc is defined by the region of First stage. This circular arc is defined by the angle that spans out between the line that goes from the starting point to center of shaft and to the tip of the nozzle outlet. As the water enters through the nozzle entry arc the first stage power is generated. The water then generally crosses the inside of the runner and leaves through the second stage, generating the second stage power. Since there is no gap between the nozzle wall and runner, flow is not entrained.

The cross–flow turbine was originally designed as a pure impulse turbine. However, modifications to the design, making the nozzle follow the runner periphery closely have given a slight positive pressure in the gap between runner and nozzle. Haimerl [12] estimated the pressure rise in the first stage of the runner to be 6.3% of the available head for large nozzle openings. The second stage operates under constant atmospheric pressure.

Velocity diagrams give an indication of the magnitude and direction of the velocity of the water. No loss through the inside of the runner is assumed, which gives equal diagrams at the outlet of the first stage and inlet of the second. In addition, an assumption of all energy extracted from the water at the turbine outlet is made, which gives no tangential component of the absolute velocity when the water leaves the runner as shown in the Figure 11.

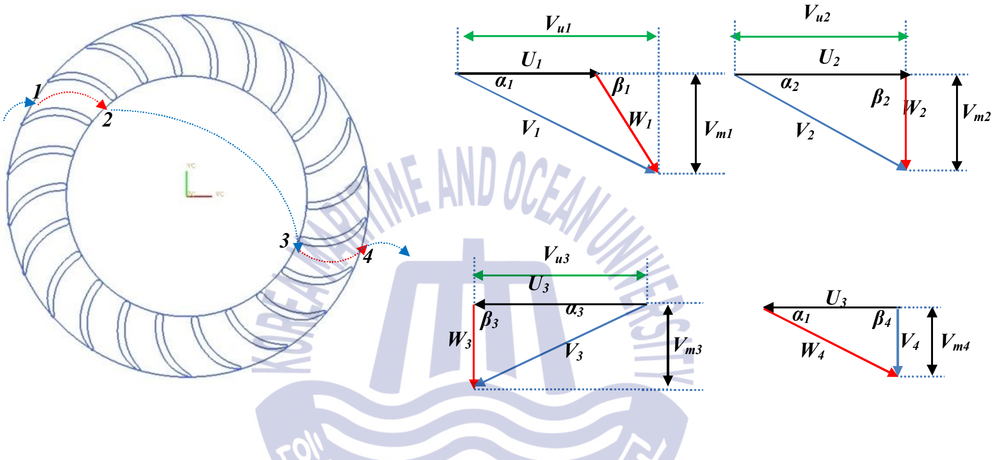

Figure 11 Velocity triangles at inlet and outlet

In Figure 11, the following notations are used:

V – The absolute velocity, *m/s*

W – The relative velocity, *m/s*

U – The peripheral velocity, *m/s*

β – Angle between relative velocity and peripheral velocity or angle between the tangents of the blade and runner periphery, *rad*

Subscript 1 – Water entering the first stage

Subscript 2 – Water leaving the first stage

Subscript 3 – Water entering the second stage

Subscript 4 – Water leaving the runner

Efficiency

The efficiency of a turbine is defined as:

$$\eta = \frac{E_u}{E_a} = \frac{E_a - loss}{E_a} \qquad \textbf{(2-1)}$$

E_u- Energy Utilized

E_a- Energy Available

When measuring the efficiency of a turbine in a laboratory one can measure the shaft torque, *Ts*, and the angular velocity, ω to enable calculation of the sum of the available energy minus the losses. When multiplying the shaft torque with the angular velocity, a direct measure of the utilized energy emerges. With these values known, the efficiency measured in the laboratory is calculated by the following equation:

$$\eta = \frac{T_s \omega}{\rho g Q H} \qquad \textbf{(2-2)}$$

T_s- Measured shaft torque, *Nm*

g – Acceleration due to gravity, m/s^2

Q – Mass flow rate, m^3/s

H- Net head, *m*

ω - Angular velocity, *rad/s*

ρ – Density of water, kg/m^3

In order to use equation 2-2, shaft torque, and rotational speed and flow rate needs to be measured. In addition, the pressure at the turbine inlet must be known to enable calculation of the net head, which is defined by equation 2-3[8].

$$H = \frac{v_1^2 - v_2^2}{2g} + \frac{\Delta p}{\rho g} + Z \qquad \textbf{(2-3)}$$

v_1- Velocity of the water at the inlet, *m/s*

v_2- Velocity of the water at the outlet, *m/s*

Δp- Differential pressure between inlet and outlet, *Pa*

Z – Difference in height between pressure transducer and center of the runner, *m*

Torque

In this section the theory behind the experiment using a strain gage is reviewed. The strain gage is utilized to find a relative measure of the torque transferred during the first and second stage of the turbine. The magnitude of torque, T, acting on a particle is defined as [21]:

$$T = F.a \qquad \textbf{(2-4)}$$

T – Torque, *Nm*

F – Force acting on the particle, *N*

a – Perpendicular distance between the line of action of a force and the axis of rotation, *m*

2.3 Literature review and previous work on the cross flow turbine

The cross–flow turbine was first invented and patented by the Australian engineer, A.G.M Mitchell in 1903. It was further developed and patented by the Hungarian Prof. Donat Banki in Germany [13]. The recognition of the turbine amplified after a series of publications between 1917 and 1919, and it became well-known for its capability to be efficient at low head with a wide range of flow. The simple design makes it cheap for manufacturing even small workshops and ease to repair at site. In contrast, Cross-flow turbines have low efficiency compared to other turbines. Nowadays the cross–flow turbine is mostly used in less–developed countries in remote area where it is out of reach from the national grids. S. Khosrowpanah, M. L. Albertson and A.A Fiuzat [14] worked on runner diameter, the number of blades, and the nozzle entry arc .The effect on efficiency on numerous head and flow rate was observed. There was a decrease in efficiency when runner diameter was reduced maintaining the same width. The maximum efficiency of each and every experiment was at the same rpm for a constant nozzle throat–width ratio. The efficiency improved with an increase in nozzle entry arc from 58° up to 90°.

Several studies, both experimental and numerical methods have been done to determine the optimal configuration of the cross- flow turbine. Most of these studies include details concerning the influence of nozzle shape. Aziz and Desai [15] conducted experiments in order to precisely identify the favorable parameters and their impact on the cross–flow turbine performance. Their research concluded that the turbine efficiency decreases with an increase of the angle of attack at the first stage from 22° to 32°. Also an increase in efficiency was observed when the number of blades increased from 15 to 30. In addition, the ratio of inner to outer diameter of the turbine did also show an effect on the efficiency of the turbine. When increasing the ratio, the maximum efficiency showed a slight reduction. Son et al. [16] conducted a numerical analysis to investigate the effect of nozzle shape on the performance of a cross- flow turbine. The results showed that relatively narrow and converging inlet nozzle shape gives better effect on the performance of the turbine. Choi et al. [17] numerically investigated the effect of turbine's structural configuration on the performance and internal flow characteristics of the cross- flow turbine model by varying the shapes of the nozzle and the runner blades. The authors concluded that the nozzle shape, runner blade angle and runner blade number are closely related to the performance of the turbine. Olgun [18] conducted an experimental investigation to study the effects of some geometric parameters of runners and nozzles (e.g. diameter ratio and throat width ratio) on the efficiency of cross- flow turbines, by varying the inner and outer diameter ratio and gate openings of two different turbine nozzles under different heads.

The turbine efficiency has been defined as the ratio between the power output and the input power in relation to machine inlet head and discharge. Previous studies show the influence of the shape of the nozzle and guide vane angle [19] on the performance of the turbine. The study has been conducted to extract the best possible efficiency modifying the curvature of the nozzle. And also the guide vane angle has been set to the point to extract the best possible efficiency. With this as the base of the study the shape of the blade has been varied according to the diameter ratio and the inlet angle considering a constant outer diameter of the turbine to study the best efficiency according to shape of the turbine.

2.3.1 Turbine setup and experiments results

The performance study of the Cross Flow turbine was initially studied in for the performance analysis for the base model through experimental analysis and numerical simulations. The model consists of 30 number blades at an inlet angle of 30° and outlet angle of 90°. The angle of attack (α) for the nozzle is at 16°. The outer diameter of the rotor is 200 mm and the ratio of outer diameter to inner diameter is 0.665. CFD simulation for the performance of the turbine was done based on the various rotational speed and flow rates to validate the result obtained from CFD simulation to that with the experiments. The result thus obtained was further improved through simulations for various design aspects such as the shape of the nozzle, guide vane angle and number of blades in simulation. This research work led the path to carry out further investigations numerically and experimentally, which has now become an integral aspect of the machinery design.

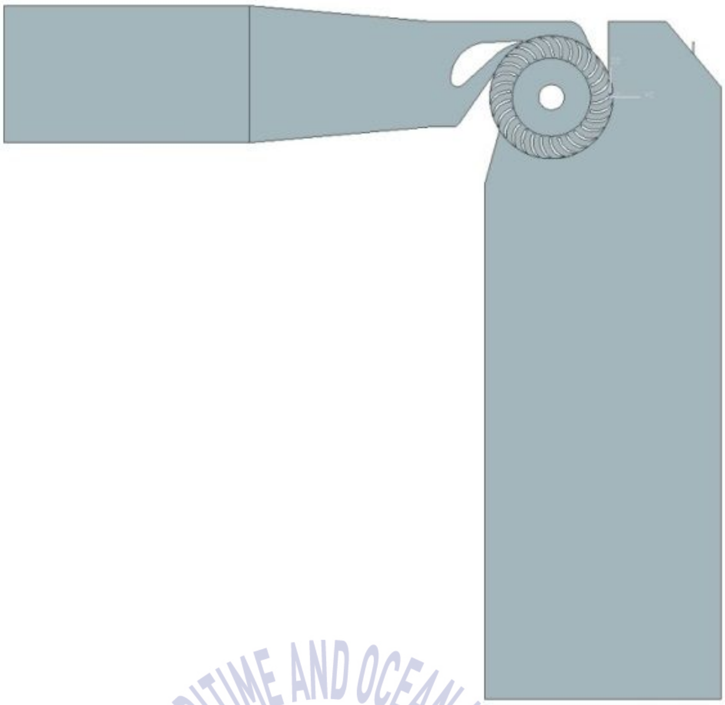

Figure 12 Turbine set up for cross flow turbine

The CFD analysis was carried out using ANSYS-CFX. The generation of the mesh in ICEM CFD, CFX setup and the result obtained from the experiment and CFD analysis are shown on the Figure 9. At the design speed of 642 rpm for full opening, experimental data show the efficiency of 61.68% whereas the numerical result shows 63.73%. The best efficiency was obtained at 500 rpm from both experiment (64.14%) and simulation (64.81%) which find good agreement with each other. [20]

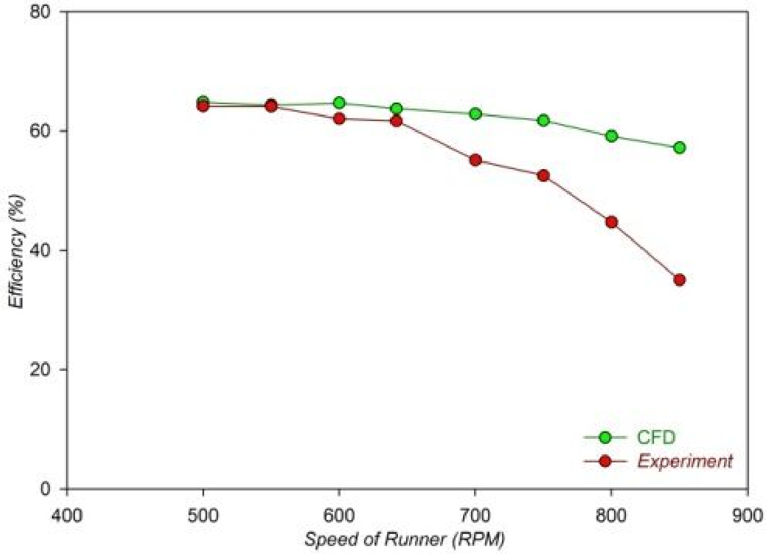

(a) Efficiency at various runner speeds

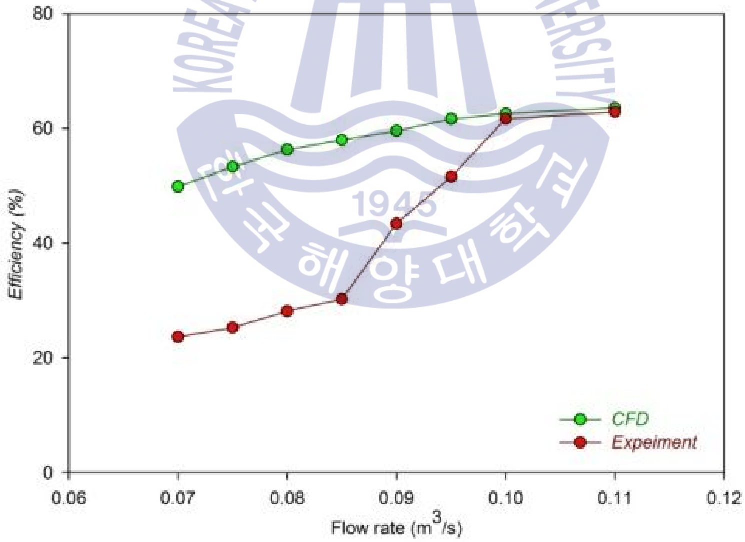

(b) Efficiency at various flow rates

Figure 13 Experimental and numerical simulation based on various runner speeds and flow rates for the base model

It was shown in the study from CFD analysis that the efficiency of the turbine showed drastic changes with the change in the shape of the nozzle and the guide vane angle positioning. Furthermore the number of blades also supports the change in efficiency positively. The simulations were done for a single runner passage, where it was shown that the runner outlet diameter, peripheral velocity at inlet, and blade angle distribution has the highest effect on the efficiency of the Cross flow turbine.

2.3.2 Design optimization and results

In the first phase of the design optimization, nozzle shape was modified. Different cases of modified nozzle with different edge blend were simulated and the results were compared with base model. Figure 14 shows the variation of base nozzle with the base nozzle. The structure of the nozzle is blend in comparison to base nozzle for reference nozzle at the curvature of 150 mm. Nozzle shape modification gives the highest efficiency of 67.26% with shaft power output of 5.48 kW compared to 4.74 kW power and 63.73% efficiency for base model. Guide Vane angle variation gives the highest efficiency of 73.09% with 7.21 kW power for 7° GV opening (0° being the full opening). Figure 15 shows the result in efficiency and power produced with all the nozzle shape modifications with specified edge blend dimensions. Varying the number of blades in the runner, the best efficiency achieved is 76.26% with 7.14 kW power for 22 blades (base runner with 30 blades) Casing length and diffuse angle variation gives the highest efficiency of 80.76% with 8.51 kW power for 750 mm long casing and 18° diffuse angle (base being 850 mm long and 0° diffuse angle) [20].

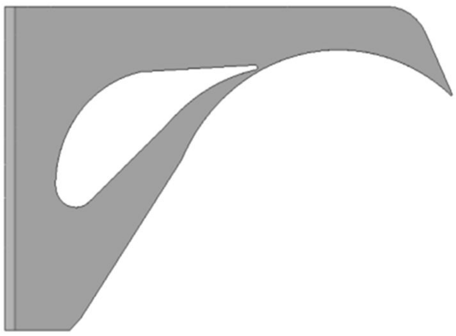

(a) Base nozzle at full open guide vane condition

(b) Blend nozzle at the curvature of 150 mm at 7° guide vane open

Figure 14 Nozzle shape variations in the base and the designed turbine

Similarly different shapes were analyzed for the nozzle blend as shown in Figure 14. It is noted that nozzle shape modification gives the highest efficiency of 67.26% as compared to 63.73% efficiency for base model. Figure 15 shows the shaft power output and efficiency of the base nozzle for the modified nozzle at various guide vanes opening. Guide vane at full open condition being at 0° and full closed at 32°. The nature of the graph illustrates that the efficiency of the turbine increases from 0° to 7° but gradually starts dropping thereafter. The highest efficiency obtained was 73.94%for 7° compared to 5.48 kW power and 67.26% efficiency for 0° GV angle.

For the current thesis the shape of the nozzle, guide vane angle and number of blades has been changed based on previous studies and the turbine setup has been constructed. The performance analysis for the new setup turbine has been conducted to study the changes in the output of the turbine in comparison to the previous turbine. Since the previous study was based on the shape of the turbine nozzle, in this thesis the study of the shape of the blades based on the inlet angle and diameter ratio has been conducted.

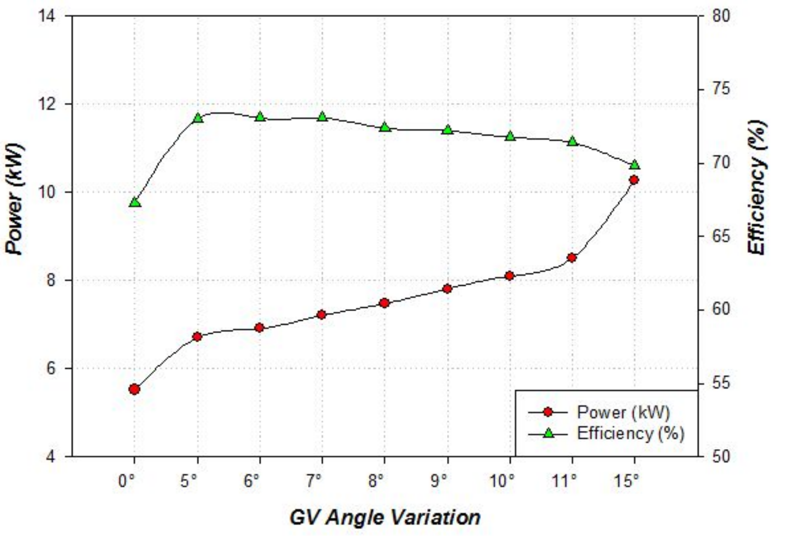

(a) Efficiency and shaft power based on various guide vane angles

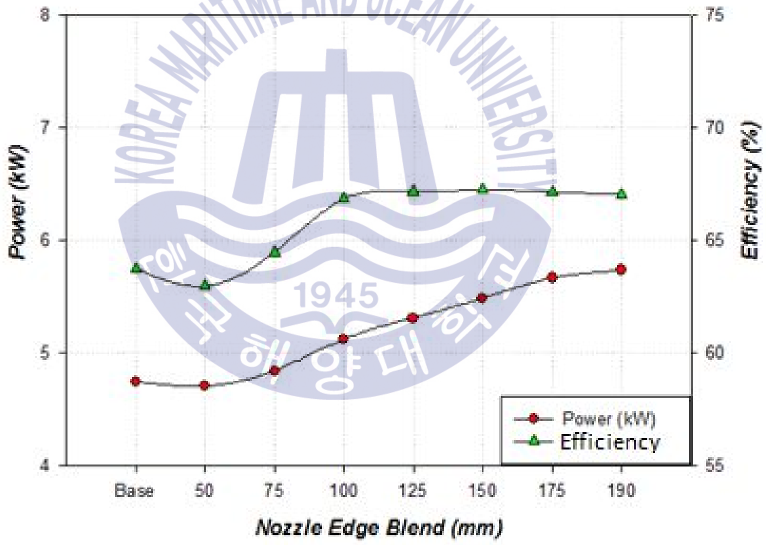

(b) Efficiency and shaft power based on variation nozzle edge blend dimensions

Figure 15 Performance characteristics at various design optimization points

3. Performance analysis and design optimization of setup turbine

3.1 Modeling

3D models of the components were generated in Unigraphics NX 6.0 according to the available designs. 200 mm outer diameter runner contains n= 22 blades with the rotational speed of 642 rpm. For the reference design, the blade is designed in way that the water enters at an inlet angle of β_1=30° and outlet angle of β_2= 90°. The reference nozzle of 150mm blend curvature contains guide vane mechanism to adjust the water flow and direction. The widths of the nozzle and runner are all same at 210mm. Air suction present in the casing [9]. The fluid domain for the CFD analysis was constructed with whole setup. No intermediate discs were considered for the CFD analysis and also for the nozzle, the whole setup with no partition was considered. Since the flow analysis was only done for the full load condition and with both the nozzle opened at the same angle.

Table 2 Turbine parameters specifications

Parameters	**Value**
Runner Diameter	200mm
Rotational Speed	642 rpm
Guide vane angle	7°
No. of Blades	22
Application	Micro Hydropower
Discharge	0.1m3/s (varied flow 0.06-0.1m3/s)
Head	10m

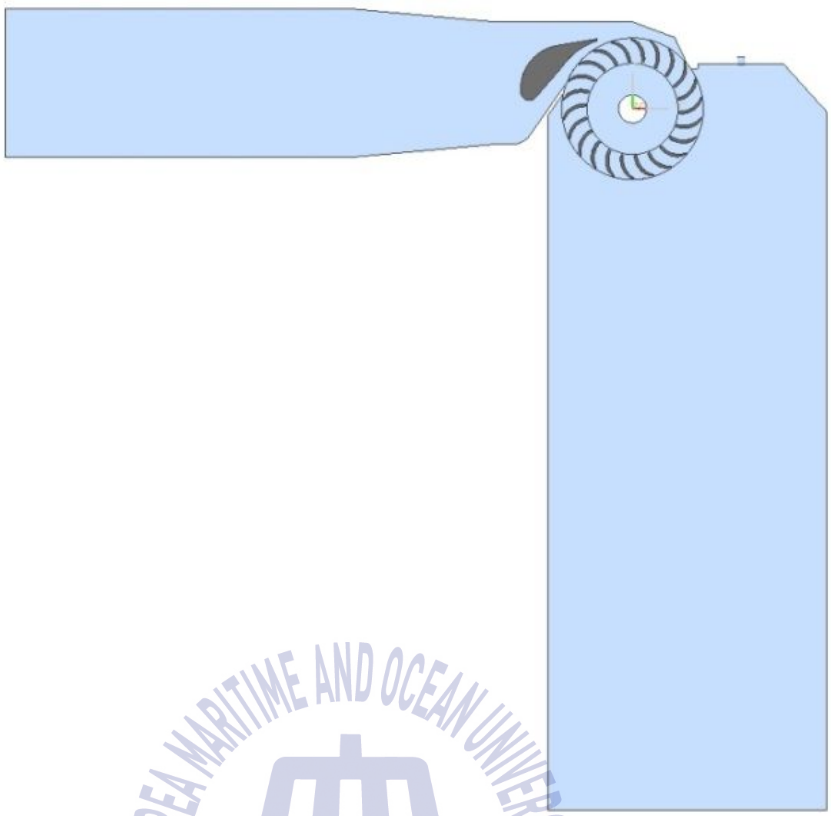

Figure 16 Modeling of fluid domain of turbine setup for CFD simulation

3.2 CFD simulations

3D steady state CFD simulations were performed using the CFD commercial code ANSYS 13.0. Fine hexahedral grids comprises of 5.5×10^6 nodes were generated in ANSYS ICEM CFD as to ensure the high accuracy of the calculated results. The inflation layer is distributed around the blade as shown in Figure 17. Quality of the mesh was verified by using a pre-processing procedure by ANSYS ICEM CFD. The simulations were conducted for the design condition Head and discharge (H, Q). Designed mass flow rate of 0.1 m^3/s at inlet and atmospheric pressure at outlet and air inlet opening valve at 0Pa at the casing were used as boundary conditions. General Grid Interface (GGI) method was used for the mesh connection between the components with the interface. Both water and air phases were modeled in the computational domain according to the free surface homogeneous model [21, 22]: according to this model the two fluids share the same dynamic fields of pressure, velocity and turbulence. In homogeneous multiphase flow, two phases coexist: water (*w*) and air (*a*). Steady state SST turbulence model [23], convergence criteria of RMS and 1x 10-5 residual were considered for maximum of 500 iterations to achieve the convergence of the solution to an acceptable level. All simulations were performed using ANSYS CFX in parallel network workstation.

Table 3 Mesh and boundary condition specification

Numerical Methods	**Mesh Type**	Hexahedral
	Mesh node number	5.5×10^{6}
	Turbulence Model	SST
	Type	2 phase Steady State
	Convergence Criteria	Max. 1e-5
	Physical timescale	1/ω
Boundary Conditions	**Rotor Stator Interface**	Frozen Rotor
	Inlet	Mass Flow Rate
	Outlet	Atmospheric Pressure
	Air Inlet	Atmospheric Pressure (Opening)
	Wall	No-slip

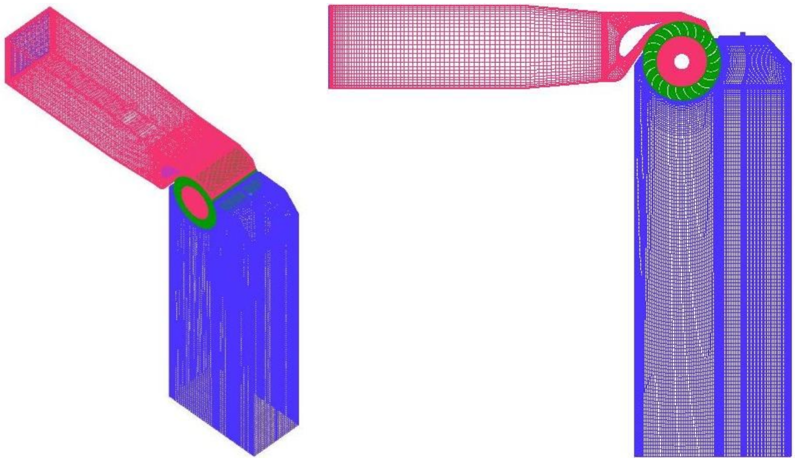

(a) For the whole setup

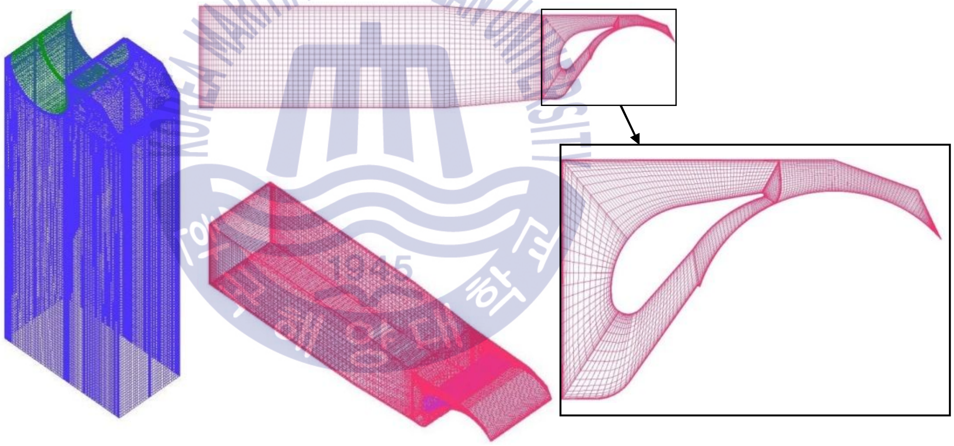

(b) Diffuser and Nozzle mesh

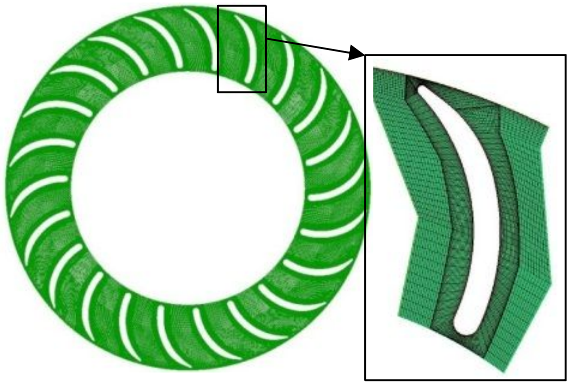

(c) Rotor mesh and enlarged portion of single blade

Figure 17 Meshing using ICEM CFD

3.3 Performance analysis of reference turbine for simulation

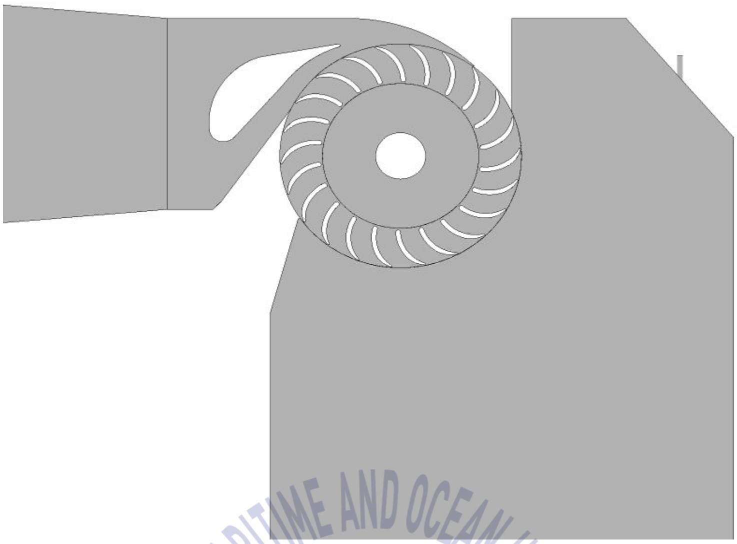

(a) Designed turbine setup

(b) Experimental turbine setup

Figure 18 CFD domains for the turbine setup

CFD simulation for the performance of the turbine has been conducted for the same turbine with two different shape of the nozzle. The nozzle manufactured has an inlet α of 16 ° whereas the one proposed considering the previous research has been of 8.8 ° as shown in Figure 18. The blades in both the turbines have been kept constant with 22 number of blades, inlet and outlet angle of 30 and 90 degrees respectively.

Similar input parameters in CFX have been used for both the cases to study their performance for the different flow rates and for the different RPM. The graph shows the value of performance of the turbines. It can be seen that the turbine

Figure 19 shows the performance of the turbine setup and the designed setup fort the various flow rates. It is seen that the performance of both the turbine increases as the flow rate of the turbine increases. It is observed that in both the cases the efficiency of the turbine was found to be best efficient at full load condition at 75.16 % for designed turbine and 71.91% for the setup turbine. The power for both the cases drops as the flow rate decreases. Head of the turbine is varied from 4.64 m at 50 kg/s to 9.5 m at full load condition.

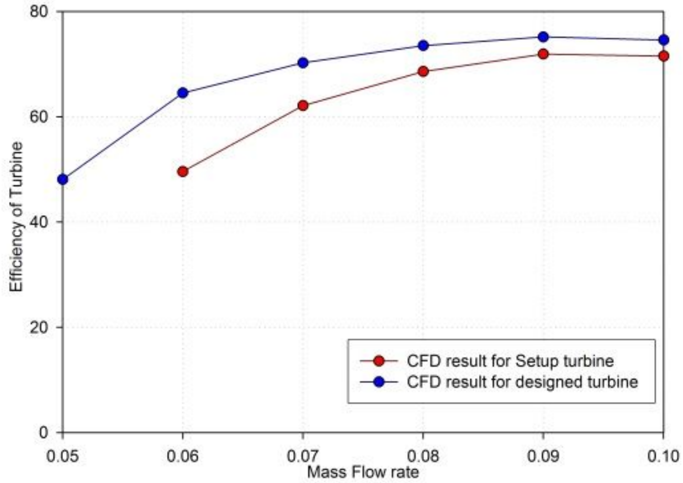

(a) Efficiency comparison for setup turbine and designed turbine

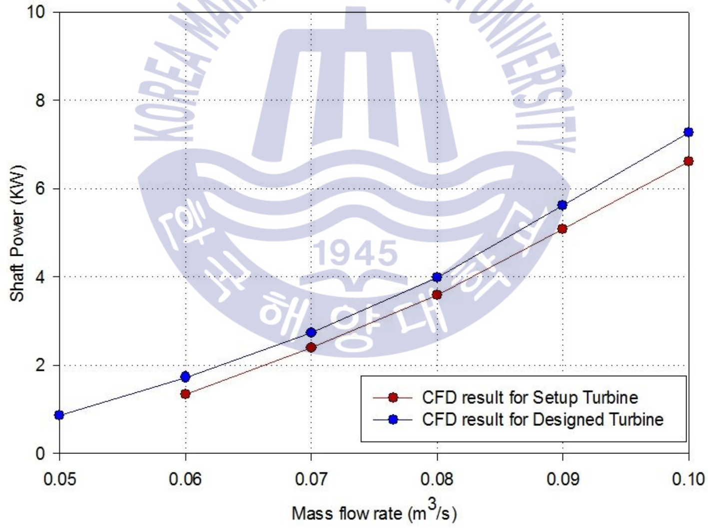

(b) Shaft power comparison for setup turbine and designed turbine

Figure 19 Performance of turbines at various mass flow rates at designed condition of 642 rpm

Figure 20 shows the performance of the turbine setup and the designed setup for the various rotational speeds. Best efficiency for the setup turbine was found for the designed rpm of 642 rpm at an efficiency of 71.9% whereas for the designed setup the efficiency was best at 750 rpm. Since the nozzle shape in the designed nozzle more efficient than that of the setup nozzle, more head can be utilized for and the result can be seen in its efficiency. For the designed turbine, 9.95 m was achieved for the 642 rpm whereas 9.47 m was obtained for the setup turbine.

It can be seen from Figure 21, the velocity vector of flow in both the turbines. It is seen that the flow velocity in the designed setup is higher in comparison to the turbine setup. Also the flow in the tip of nozzle is much smoother than that for the setup model. The flow in the recirculation zone in region 1 is also much less in comparison to other turbine. This has been the major causes for the performance enhance in the design turbine as compared to setup turbine.

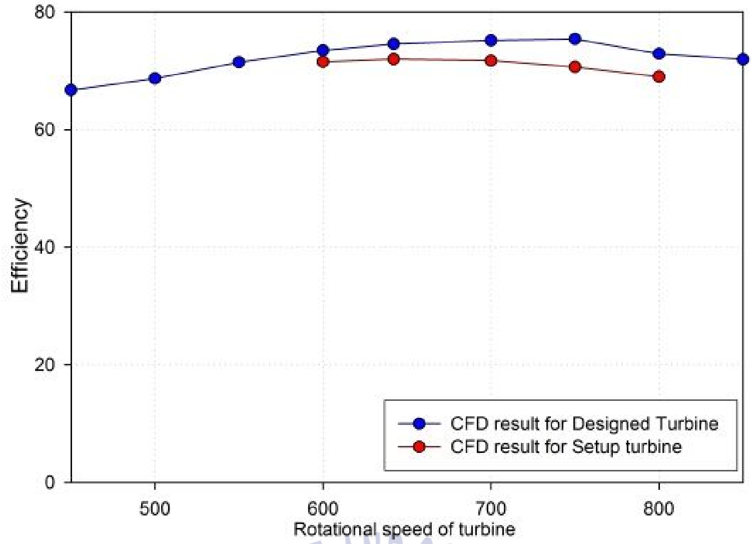

(a) Efficiency comparison for setup turbine and designed turbine

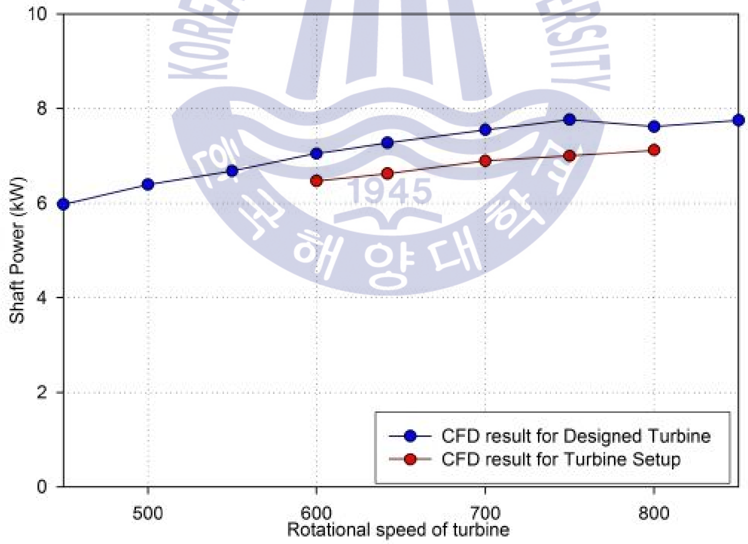

(b) Shaft power comparison for setup turbine and designed turbine

Figure 20 Performance of turbine at various rotational speeds at designed condition 0.1 m3/s flow rate

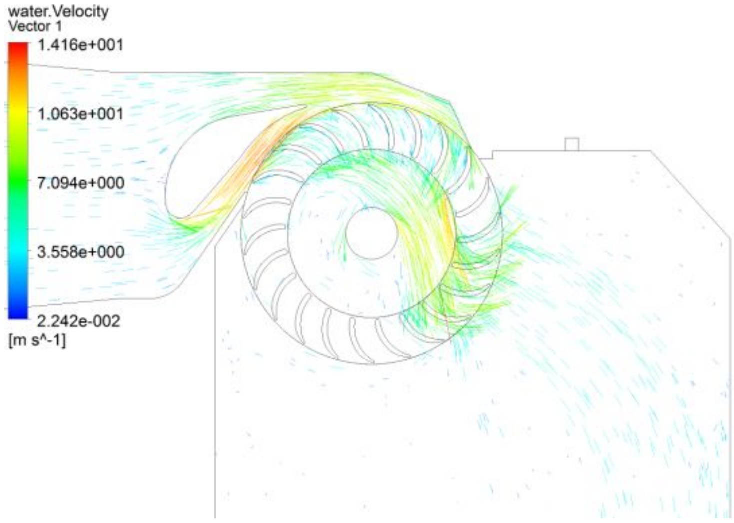

(a) Turbine setup

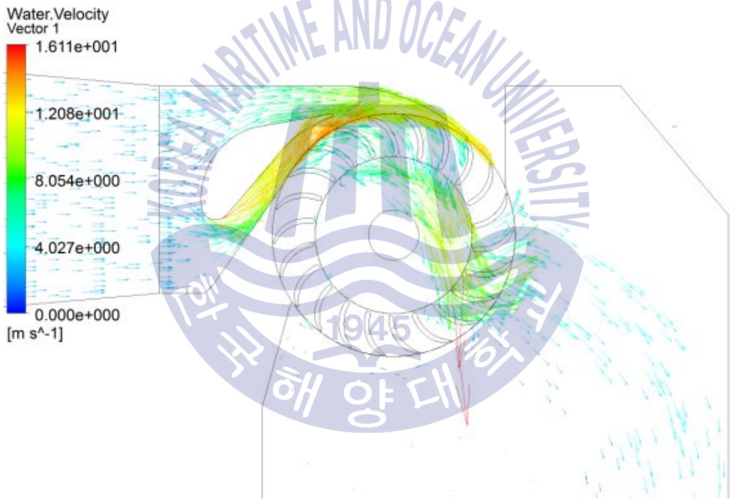

(b) Designed setup

Figure 21 Velocity vector comparisons for setup and designed turbines

3.4 Experimental equipment and test procedures

3.4.1 The turbine

A 3D–model of the cross–flow turbine used in the experiments is shown in Figure 22. This cross–flow turbine consists of a steel casing, an adjustable nozzle and a runner. The turbine casing is made out of steel plates which are bolted, giving a high strength. The nozzle has a rectangular shape, with an adjustable guide vane. The wheel mounted on top of the turbine regulates the nozzle opening. The nozzle entry arc on this turbine is 7°. The runner consists of 22 blades symmetrically arranged between four circular plates along the plate periphery. The shape of the blades, which is shown in Figure 22, is circular. The blades have an inlet angle, β_1 of 30° and an outlet angle, β_2 of 90°.

There is a two compartment for water flow. Both of these water compartments in nozzle has been kept open at an angle at 7 degree for the studies and both the guide vane angles are opened in the same angle for the study of the flow.

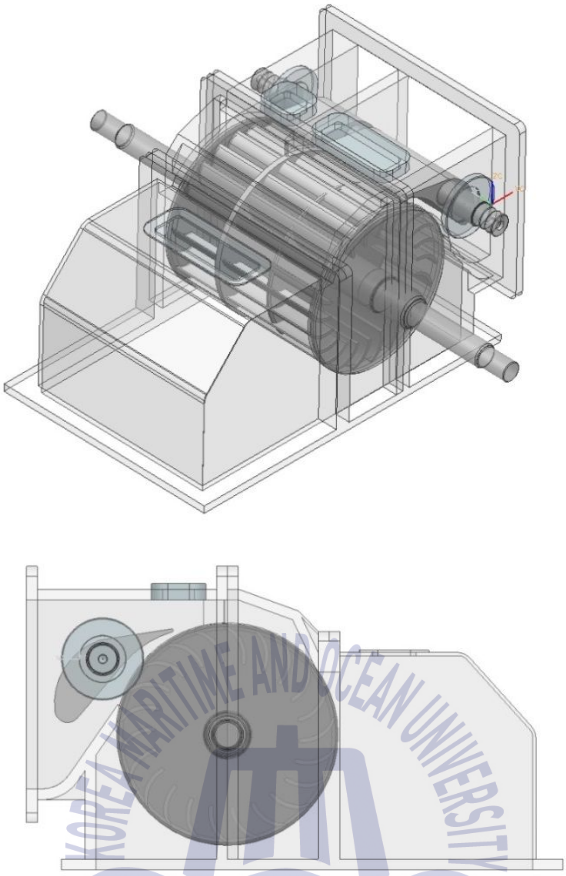

(a) Turbine setup

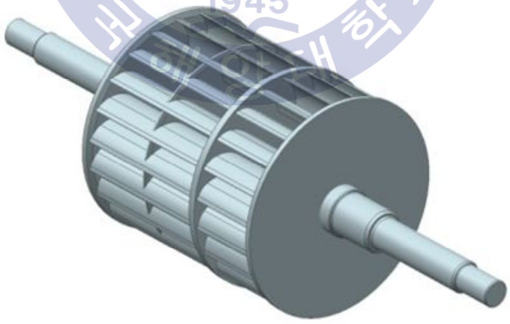

(b) Turbine runner with intermediate disc

Figure 22 3D modeling for the experimental setup

3.4.2 Installation

The turbine was connected to a closed surface loop in Fluid Laboratory in Korea Maritime and Ocean University. The closed surface loop, which is shown in Figure 23, can provide a maximum of 10 meter head. A pool of water is located just below the turbine outlet. Variable Frequency Drive (VFD) was started which controls the rpm of the pump, which helps to maintain the required head. A pump pumps water from the pool up to the pipe loop. The butterfly valve present in the pipeline regulates the flow in the pipe. A valve located upstream the turbine is used to regulate the head in a range of 5 -14 meter. After the turbine outlet the water goes directly back into the pool. As soon as the turbine started rotating, air trapped inside the pipeline was drained out and the water supply valve to the powder brake was done immediately (water- cooled type powder brake). The tension controller was started and thus the rpm of the turbine was controlled as required. The required parameters were recorded in the data logger and the data obtained were used for performance analysis.

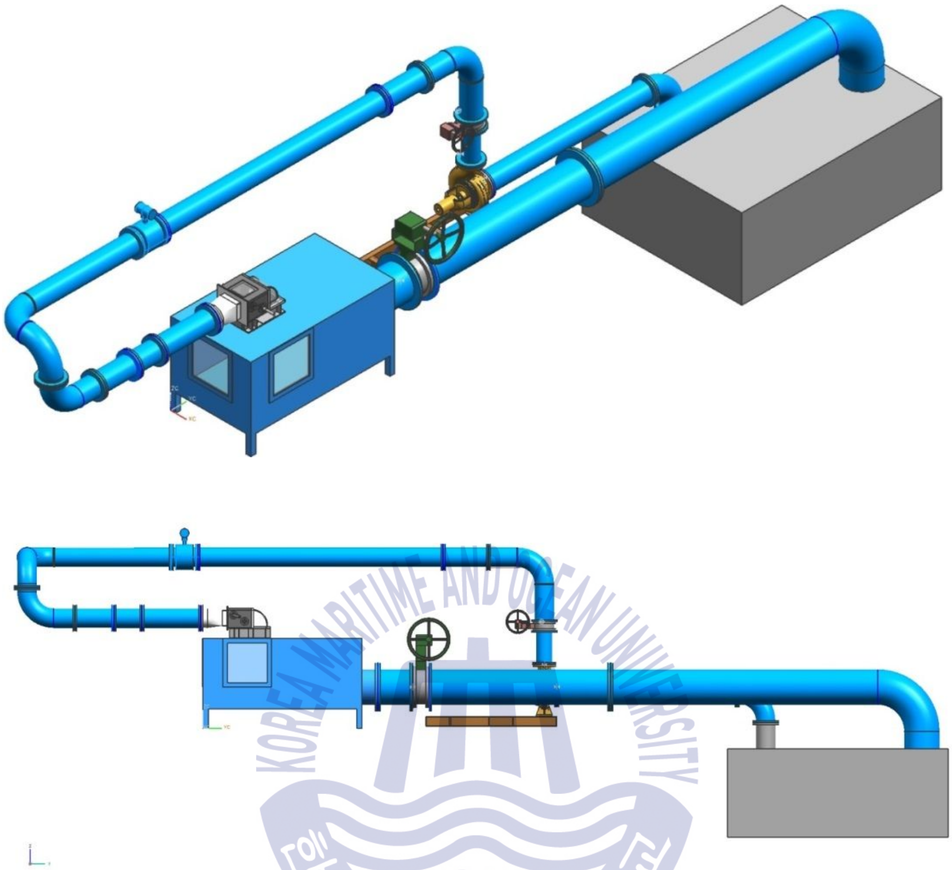

Figure 23 3D drawing for experiment setup

Figure 24 Laboratory turbine setup

Figure 25 Overall arrangement of the setup

Table 4 Equipment used with their specifications

Equipment	Specification
Pump	Head: up to 10m Power: 25 HP N: 1750 rpm
Pitot Tube	Model 167-6-CF, Insertion Length: 6”
Pressure Transducer	Range: 760~ 760mmHg O/P: 1~5 VDC
Torque Transducer	SBB-5K.
Powder Brake	Model: Pora PRB Y3
Data Logger	Model: Powertron- t=1624

3.4.3 Instrumentation

Pitot tube

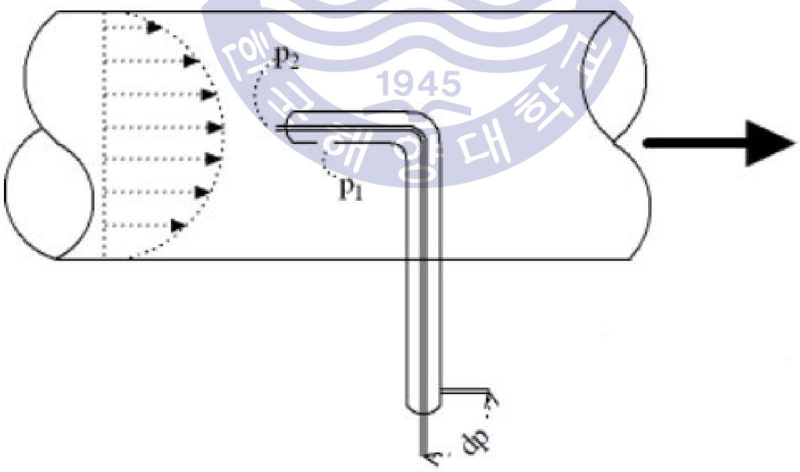

Figure 26 Pitot tube

A pitot tube is used to determine the velocity of a fluid flowing through a pipe. It works by using a manometer-like attachment to measure the difference in pressure between two points in a pipe, which makes it possible to determine the velocity of the fluid in the pipe using Bernoulli's equation. It can vary the density of the fluid in the manometer for appropriate ranges of fluid velocities and manometer heights. It is also noted that the height and velocity scales are different for the two options

$$\boldsymbol{P_2 = P_1 + \rho v^2} \qquad \textbf{(3-1)}$$

$$\boldsymbol{v = \sqrt{\frac{2(P_2 - P_1)}{\rho}}} \qquad \textbf{(3-2)}$$

$$\boldsymbol{Q = A \times v} \text{ ; } \textbf{Where} \qquad \textbf{(3-3)}$$

P_2 is stagnation pressure and P_1 is pressure at the open section

ρ is density of water,

v is velocity of water,

Q is the mass flow rate and

A is the area of the cross section of the penstock pipe

Pressure Transducers

The experimental setup consists of three circumferential pressure tapings specifically to measure pressure at the turbine inlet, turbine outlet, separator inlet and separator outlet (overflow). The SENSYS pressure transducers of measurement capacity up to 300 kPa were installed in the setup pipeline. Two pressure transducers were arranged with Pitot tube for measurement of the velocity at the pipeline. The other transducer was used in the turbine inlet. The head calculated was based on the inlet pressure of the turbine using equation (3-4).

$$H = \frac{P_{inlet}}{\rho g Q} \tag{3-4}$$

Where

H is the Head at the inlet,

P_{inlet} is the Pressure measured from Pressure transducer at inlet,

ρ is the density of water and

Q is the mass flow rate measured from the Pitot tube

Torque transducer

The turbine was equipped with a torque transducer with an inbuilt RPM and torque sensor. The use of strain gauge with brush and slip ring in the transducer produces measurement with high accuracy. The applications of the transducer include test of motor power, test of load speed reducers, test of brakes and clutches, test of nut and bolt tightening torque calculation and also test of brake properties. The torque transducer consists of shaft open at both ends. One end of the shaft was coupled to the powder brake shaft while other end was coupled to the turbine shaft. A flexible jaw coupling was used to couple the shafts. Jaw coupling are designed to transmit torque while damping system vibrations and accommodating misalignment which protects other components from damage.

The torque transducer used in the experimental analysis is a shaft type torque transducer. The model number of the torque transducer is SBB-5K.

Figure 27 Torque transducer

Powder brake

An electromagnetic braking device also known as powder/ particle brake is used in the experimental analysis to apply load on the turbine and dissipate the power generated as heat energy. Magnetic particle brakes are unique in their design from other electro-mechanical brakes because of the wide operating torque range available. Like an electro-mechanical brake, torque to voltage is almost linear; however, in a magnetic particle brake, torque can be controlled very accurately (within the operating RPM range of the unit).

Magnetic particles (very similar to iron filings) are located in the powder cavity. When electricity is applied to the coil, the resulting magnetic flux tries to bind the particles together, almost like magnetic particle slush. As the electric current is increased, the binding of the particles becomes stronger. The brake rotor passes through these bound particles. The output of the housing is rigidly attached to some portion of the machine. As the particles start to bind together, a resistant force is created on the rotor, slowing, and eventually stopping the output shaft. When electricity is removed from the brake, the input is free to turn with the shaft. Since magnetic particle powder is in the cavity, all magnetic particle units have some type of minimum drag associated with them.

Figure 28 Powder brake

The model number of the powder brake used in the analysis is PRB-5Y_3F.The powder brake was coupled to the torque transducer using jaw coupling.

Based on the obtained pressure differences the velocity of the water is measured in the penstock. Then the flow rate at such point is obtained as the product of the velocity at that point and area of the cross section of the pipe. With the obtained outputs, the program is constructed in data logger. Its program collects signals from the measuring instruments and calculates the required parameters of the turbine.

3.4.4 Experimental results for the variation for rotational speed

The tests are performed with a constant head of 10 m, and nozzle openings of 7°. For each opening the rotational speed varied between 600 rpm and 800 rpm. These values were decided based on numerical simulations that showing that the best efficiency point for 10 m head occurs with a rotational speed of approximately 642 rpm. After processing the data from the flow visualization experiments, the general flow patterns through the turbine for different nozzle openings was drawn. This speed is chosen based on the efficiency measurements that were performed during the experiments. The results showed that for the nozzle openings of 7°, had their best efficiency at this rotational speed. Figure 29 presents an overview of the efficiency measured for each rotational speed and nozzle opening tested. It is observed the best efficiency of 69.4% was obtained for the designed rpm of 642 rpm but the efficiency was not much difference as compare to 600 rpm at 69.3%. As the rotational speed of the turbine increases the efficiency and the power output gradually decreased.

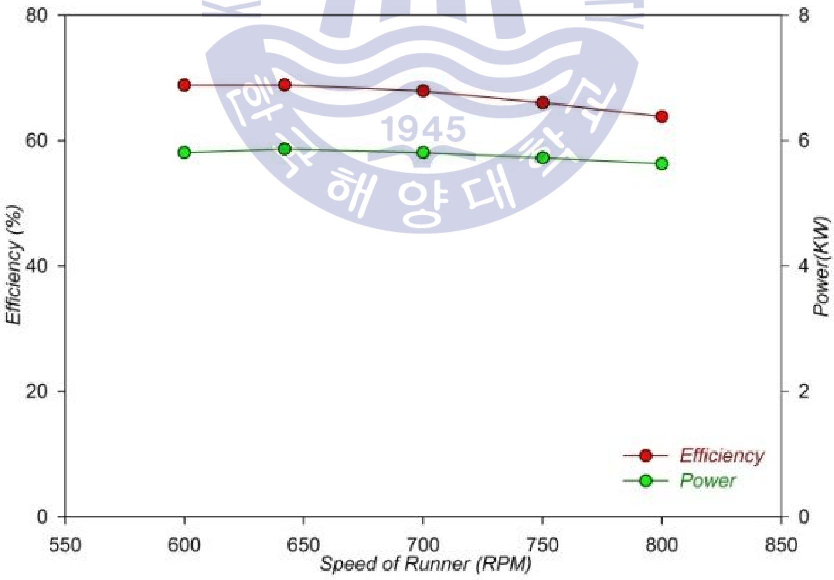

Figure 29 Performance of turbine for various rotational speeds

3.4.5 Experimental results for the various flow rates

Another case of tests were performed with a constant head of 10 m, and nozzle openings of 7°. For each the rotational speed was kept constant for the best efficiency value of 642 rpm and the test were done for the variation of the flow rate varied for 60% to 100% of total flow. After processing the data from the flow visualization experiments, the general flow patterns through the turbine for different nozzle openings was drawn. This speed is chosen based on the efficiency measurements that were performed during the experiments. The results showed that for the nozzle openings of 7°, had their best efficiency at this rotational speed. Figure 30 presents an overview of the efficiency measured for each rotational speed and nozzle opening tested. From the experiment it is observed the best efficiency of the turbine was obtained for the designed load condition of 100 kg/s. The performance of the turbine gradually decreases as the flow rate decreases. It is observed that the efficiency of 50.5 % was found at the 60% of the flow rate.

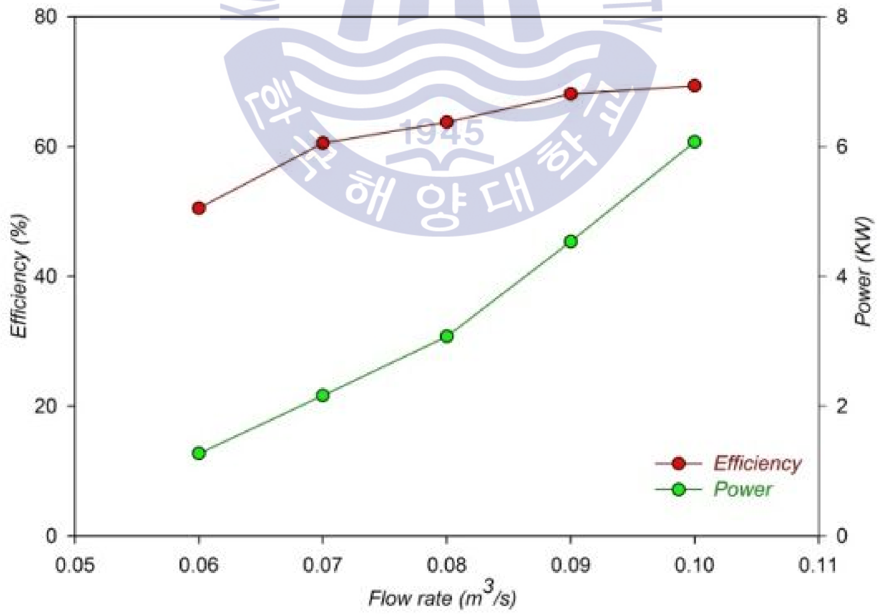

Figure 30 Performance of turbine for various flow rates

3.4.6 Experimental results for various guide vane angles

Another case of tests were performed with a constant power output of 5 kW, and varying the nozzle openings of 7° to 15°. For each the rotational speed was kept constant for the best efficiency value of 642 rpm and the test were done for the variation of the flow rate constant at 100% of total flow. After processing the data from the flow visualization experiments, the general flow patterns through the turbine for different nozzle openings was drawn. This speed is chosen based on the efficiency measurements that were performed during the experiments. The results showed that for the nozzle openings of 7°, had their best efficiency at this rotational speed. Figure 31 presents an overview of the efficiency measured for each guide vane angle and the power output at such points. The head of the turbine varied from 8 m to 12.40 m as the nozzle guide vane was angle was increased. The efficiency of the turbine ranges from the 57.4% for 15° opening to 69.4% for full open condition at 7°

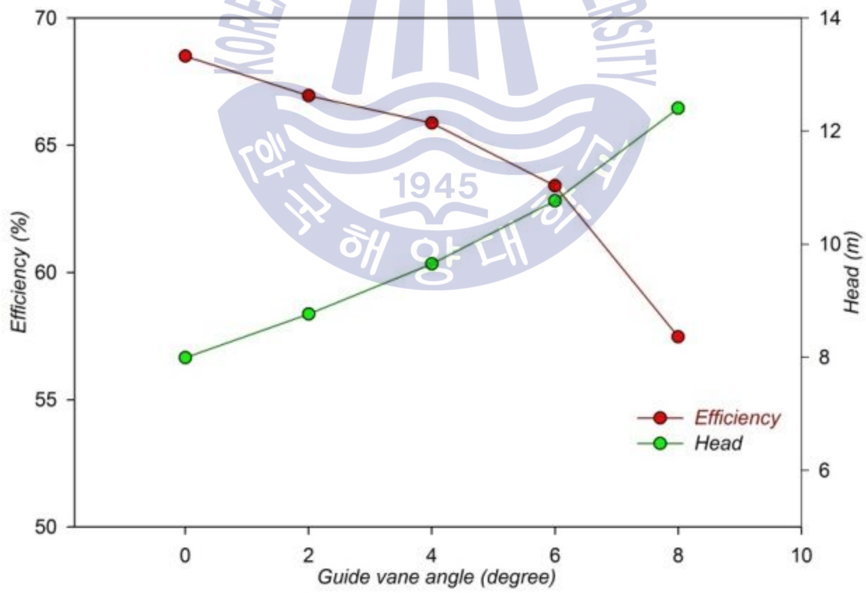

Figure 31 Performance of turbine for various guide vane angles keeping power output constant at 5 kW

3.5 Comparison of experimental and CFD simulation results

The performance analysis of the turbine was based upon the performance of turbine based on the numerical simulation and the validation of the result based on the result of the experiments. The following graph shows the result comparison in between the experiment performed as compared to the designed turbine and the result based on the CFD result obtained for the setup.

It can be seen that the result obtained from the experiment is in close approximation to the result obtained with the numerical simulation. The best efficiency point obtained for the experiment and the numerical simulation is at the design rpm at the load condition at efficiency of 69.4% and at 90% load condition 71.9%. The design condition for the setup was at 73.95% obtained through the CFD simulations. The pattern of the graph is similar as the speed of the turbine is changes. The result from the graph shows the setup simulation and experimental setup shows same value at 0.06 and 0.07 m^3/s flows.

It is observed, that the best efficiency for the setup design experimentally and numerically was at the designed speed of 642 rpm. It is observed that as the speed of the turbine increases there is a gradual loss in the efficiency of the turbine. However in case of designed setup the efficiency of the turbine was best achieved at the rpm of 750 but the design head achieved was 10.49 m which exceeded the design head of the turbine.

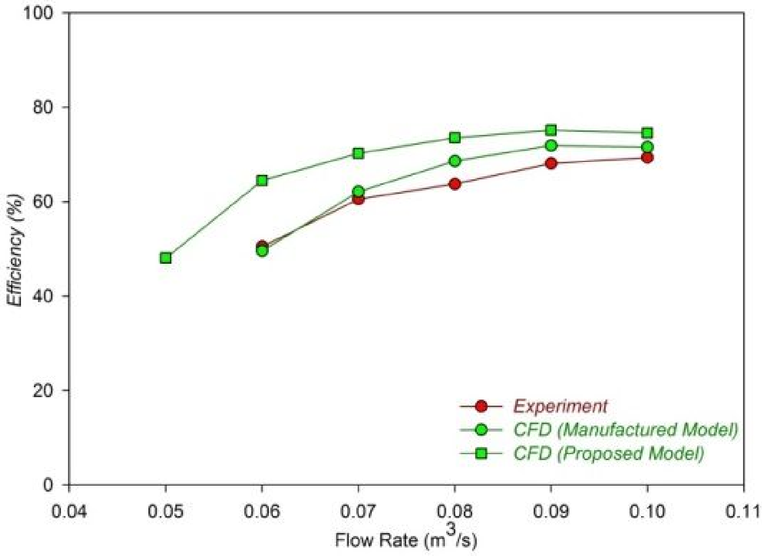

(a) Efficiency comparison for numerical and experimental results

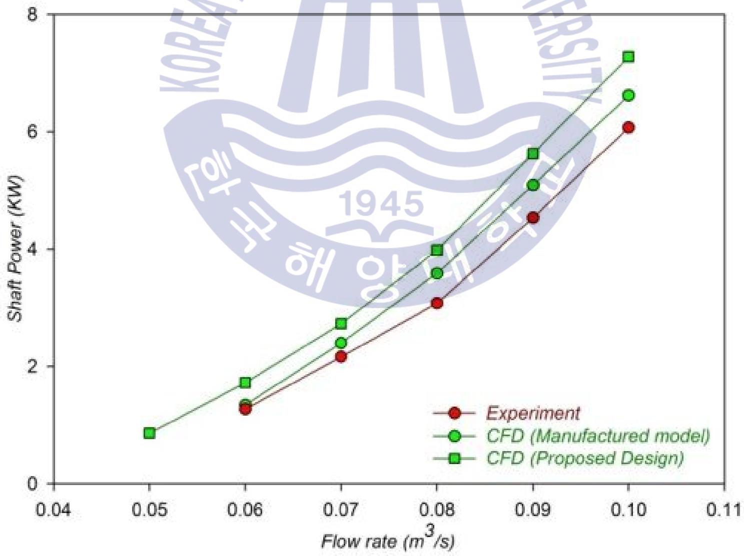

(b) Shaft power comparison for numerical and experimental results

Figure 32 Comparison of experimental and CFD results for various flow rates

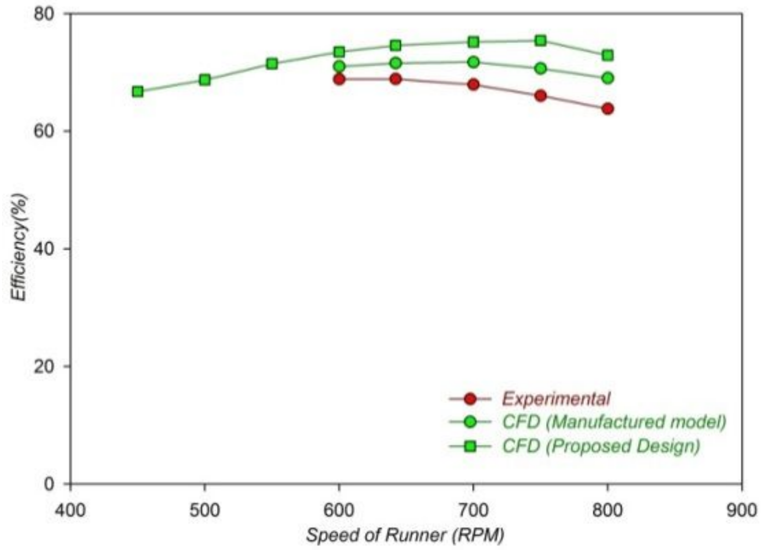

(a) Efficiency comparison for numerical and experimental results

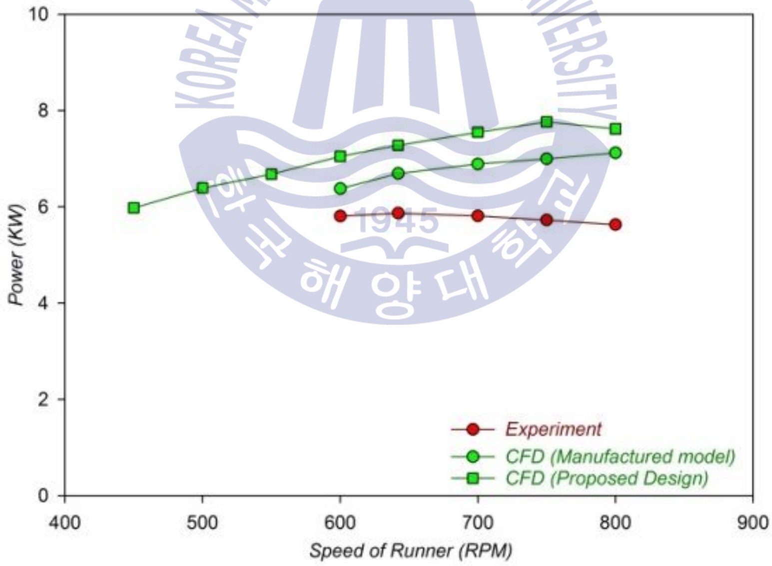

(b) Shaft power comparison for numerical and experimental results

Figure 33 Comparison of experimental and CFD results at various rotational speeds

3.6 Experimental result comparison for base turbine and setup turbine

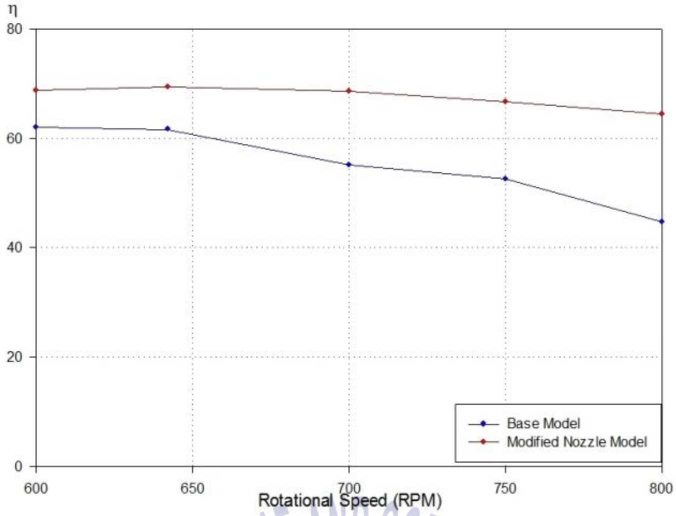

(a) Efficiency comparison at various rotational speeds

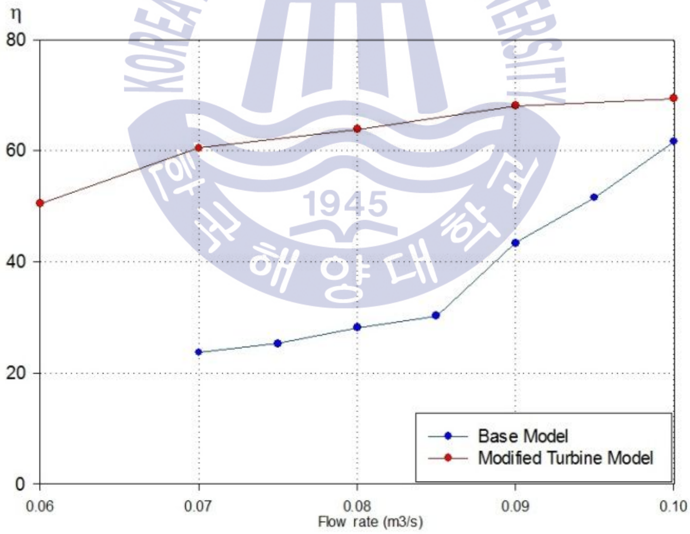

(b) Efficiency comparison at various flow rates

Figure 34 Experimental evaluations for the performance of base turbine and modified turbine at various rotational speeds and flow rates

Figure 34 shows the experimental evaluation for the performance of the base turbine with modified turbine. The result can be seen in the improvement in the performance of the turbine in comparison to base turbine as well as the overall performance at different flow rates and flow has been improved.

It shows the efficiency of the turbine has been increased from 61.7% from the previous turbine to 69.4% experimentally. Also the performance of the turbine for the different flow rates for the previous turbine shows the performance fluctuation as the performance drops immediately after the best cases, but for the modified cases the performance of the turbine drops gradually in comparison and the drop in performance is gradual. Its shows the performance of the cross flow turbine for different flow rates to be as of cross flow turbine.

3.7 CFD simulation for the change in blade with respect to the diameter ratio

The diameter ratio of the cross flow turbine is for the turbine inlet diameter and the turbine outlet diameter. The best efficiency for the turbine ratio diameter is found to be around 0.68. The diameter ratio for the test turbine is 0.665. For this study the outer diameter of the turbine has been kept constant at 200 mm and the inner diameter has been varied to obtain the various diameter ratios. Various diameter ratio sizes for the turbine have been studied using the numerical simulation to find the best efficiency. The result is presented in the graph below. It is seen that the best efficiency of the turbine has been obtained for the diameter ratio of 0.7% at 75.66%. Increase in diameter ratio, corresponds the increase in curvature of the blade. For the reference nozzle of 0.665 diameter ratio, power output of 7.03 at 73.95% efficiency is obtained. Maximum efficiency of 75.66% and 7.1 kW was obtained at 0.7 diameter ratio. However, there weren't many changes in efficiency of the turbine for the change in diameter ratio from 0.68 to 0.72.

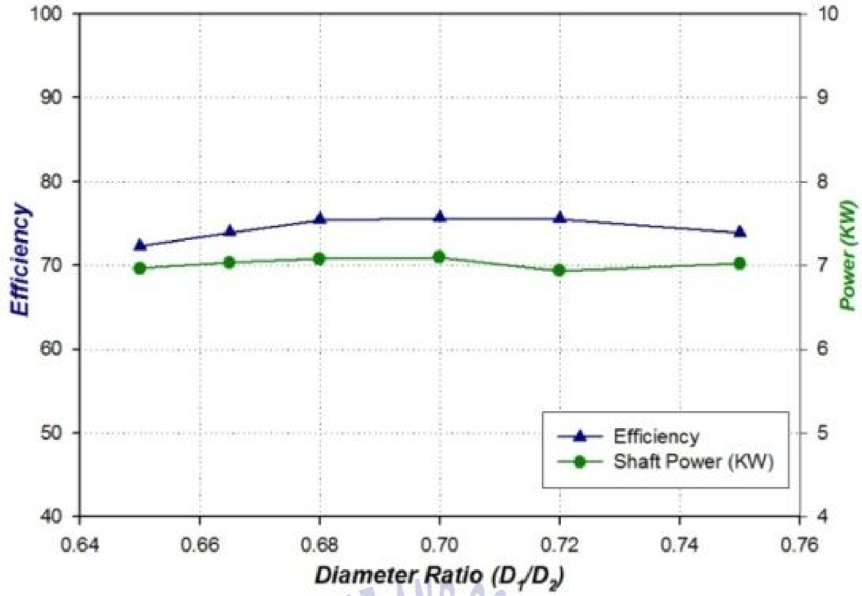

Figure 35 Performance of turbine at various diameter ratios at designed condition of 642 rpm and 0.1 m^3/s flow rate

Figure 36 indicates stage of the flow region. Hence divided power output is calculated at each region of the runner blades. Figure 36 presents the divided local output powers at each region of the runner blades. The local output power is evaluated from the calculated local output torque at each region of runner blades. Negative power output is observed in Region 1. Remarkable output power loss occurs in the Region 1 i.e. the recirculation area. Therefore, supply of proper air flow rate to form the air layer in the runner passage can improve the turbine performance considerably. It is observed that the losses in these regions are reduced with the change in diameter ratio. It is shown from the radial plot for the cases the peak torque is achieved at stage 1. As the diameter ratio increases the peak torque at the end of stage 1 decreases and the torque is distributed throughout stage 2. Maximum negative torque achieved at the end of stage 1 as shown in Figure 36 for 0.65 diameter ratio.

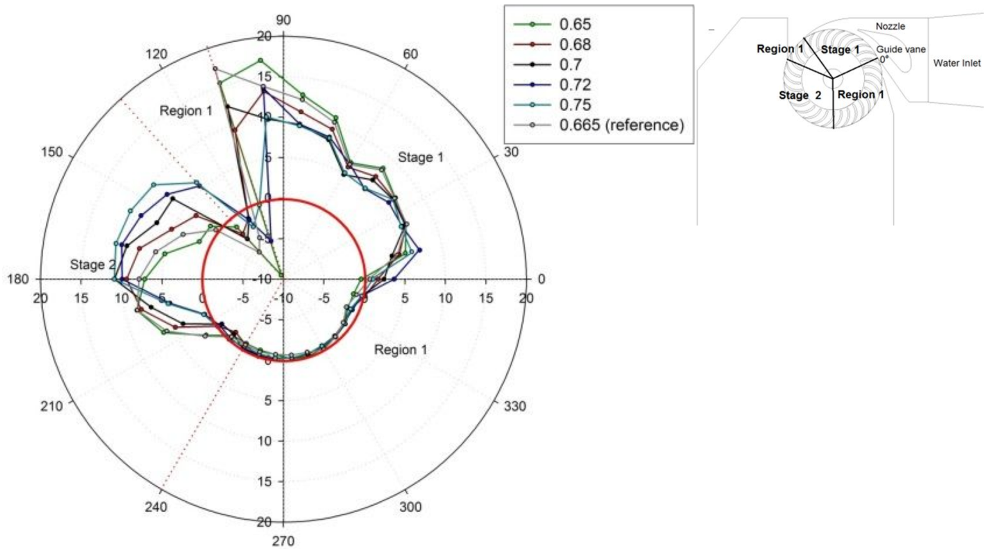

Figure 36 Performance at various diameter ratios at different stages for the designed condition of 642 rpm and 0.1 m^3/s flow rate

Figure 37 shows velocity vectors in the internal flow field of the turbine model by the variations of diameter ratios and blade inlet angle respectively. The fluid velocity becomes accelerated along the nozzle passage from the inlet. After passing through the runner blade passage at Stage 1, cross-flow within the runner center gains accelerated velocity and then the flow enters into the inlet of Stage 2. It is seen from the velocity vectors the presence of recirculation zone in reference design as compared to modified design. The change in the diameter ratio contributes in less recirculation flow. As it is show in Figure 37, the power losses in the recirculation zone decreases over the changes.

Figure 37 shows velocity vectors in the internal flow field of the turbine model by the variations of diameter ratios and blade inlet angle respectively. The fluid velocity becomes accelerated along the nozzle passage from the inlet. After passing through the runner blade passage at Stage 1, cross-flow within the runner center gains accelerated velocity and then the flow enters into the inlet of Stage 2. It is seen from the velocity vectors the presence of recirculation zone in

reference design as compared to modified design. The change in the diameter ratio and blade angle contributes in less recirculation flow.

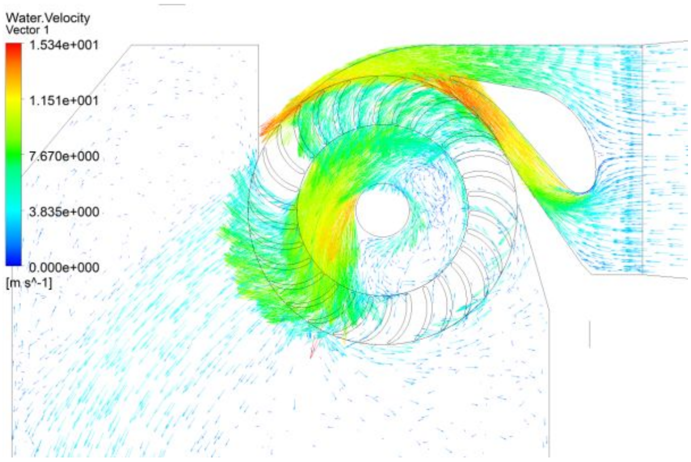

(a) 0.665 (Reference)

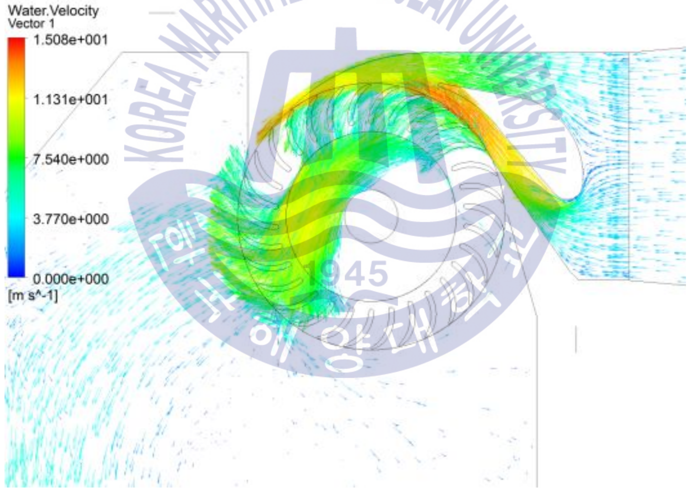

(b) 0.7 (Designed condition)

Figure 37 Velocity vectors for different diameter ratio at the designed condition of 642 rpm and 0.1 m^3/s flow rate

3.8 Distribution based on the shape of the inlet angle of the blade

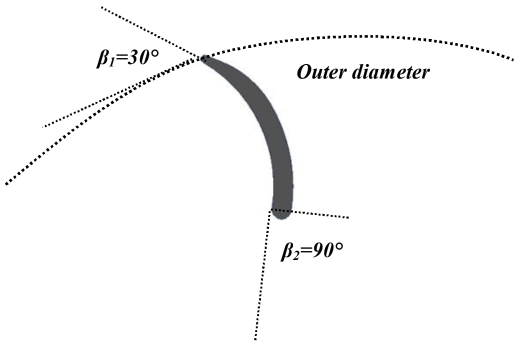

Figure 38 Blade geometry

The shape of the blade is changed based on the inlet angle as shown in the Figure 38. The inlet angle of the blade is varied from 15° to 38°. The change in the shape of the nozzle with edge blend has considerable changes in the angle of attack. The following relationship between α and β_1 is used to obtained the inlet angles. [24]

$$Tan\beta_1 = 2 \cdot Tan\alpha \tag{3-5}$$

Figure 39 shows the efficiency and power comparison based on the various inlet blade angles. The diameter ratio for this calculation is similar to the base turbine of 0.665 and the outlet blade angle *(β_2)* is constant at 90° and inlet angle has been varied. For the reference design, power output of 7.03 kW at efficiency of 73.95% was achieved. Since the nozzle curvature was changed with respect to base design, the angle of attack at the nozzle outlet decreases accordingly. As per equation (3-5), to improve the performance of the turbine the blade inlet angle has been decreased. It shows in Figure 39 that as the inlet angle decreases the efficiency of the turbine increases. The efficiency increased till the inlet angle was reduced till β_1=20° at the efficiency of 77.5% and power of 7.5 kW and for further less the efficiency decreases gradually. The efficiency of the turbine can be increased up to 78.90% for the β_1=20° and diameter ratio of 0.70.

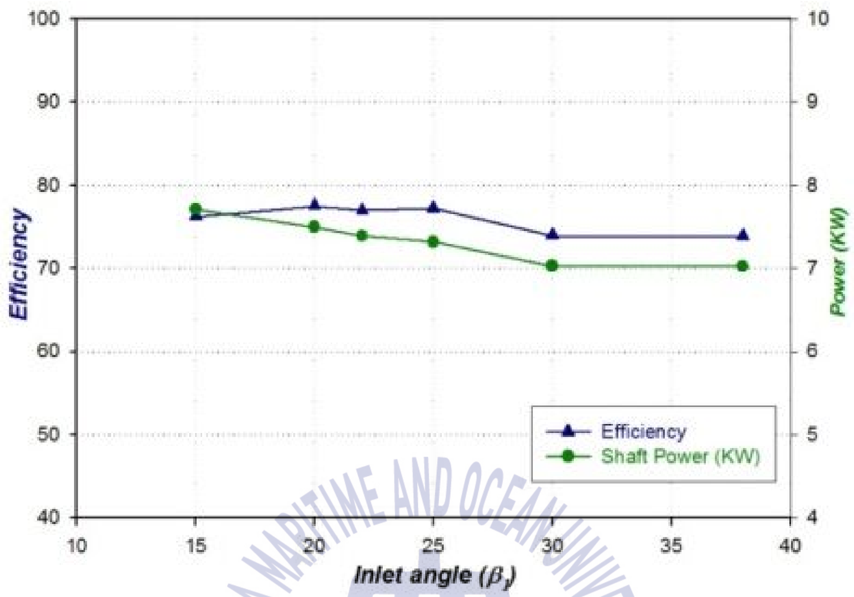

Figure 39 Performance at various inlet angles at designed condition of 642 rpm and 0.1 m^3/s flow rate

Figure 40 indicates stage of the flow region. Hence divided power output is calculated at each region of the runner blades. The graph shows the torque at each blade. It is shown from the radial plot for the cases the peak torque is achieved at stage 1. As the inlet angle decreases the maximum torque at the end of 1st stage decreases but the torque in 2nd stage is evenly distributed. The peak torque at the end of stage 1 decreases and the torque are distributed throughout stage 2.

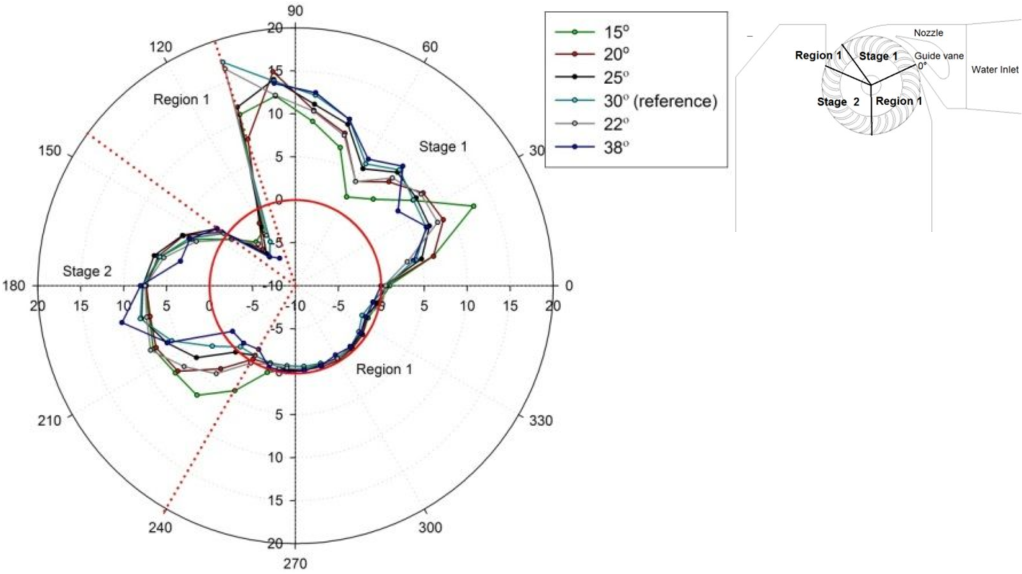

Figure 40 Performance at various blade inlet angles at different stages for the designed condition of 642 rpm and 0.1 m^3/s flow rate

Figure 41 shows velocity vectors in the internal flow field of the turbine model by the variations of diameter ratios and blade inlet angle respectively. The fluid velocity becomes accelerated along the nozzle passage from the inlet. After passing through the runner blade passage at Stage 1, cross-flow within the runner center gains accelerated velocity and then the flow enters into the inlet of Stage 2. It is seen from the velocity vectors the presence of recirculation zone in reference design as compared to modified design. The change in the diameter ratio contributes in less recirculation flow. As it is show in Figure 41, the power losses in the recirculation zone decreases over the changes.

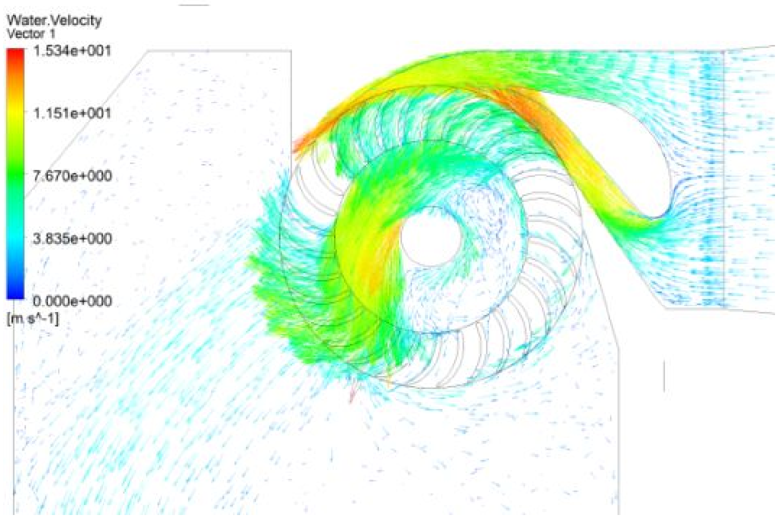

(a) 30° (Reference)

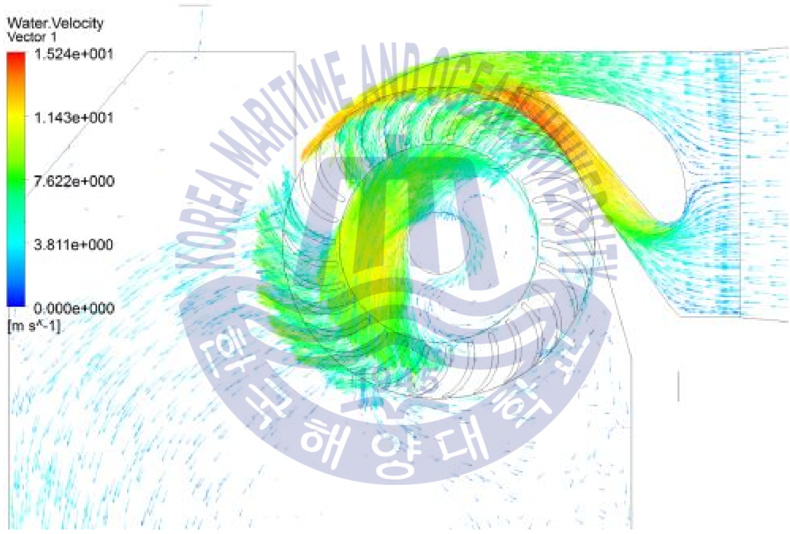

(b) 20° (Designed condition)

Figure 41 Velocity vectors for different inlet angle at the designed condition of 642 rpm and 0.1 m^3/s flow rate

3.9 Performance at various numbers of blades

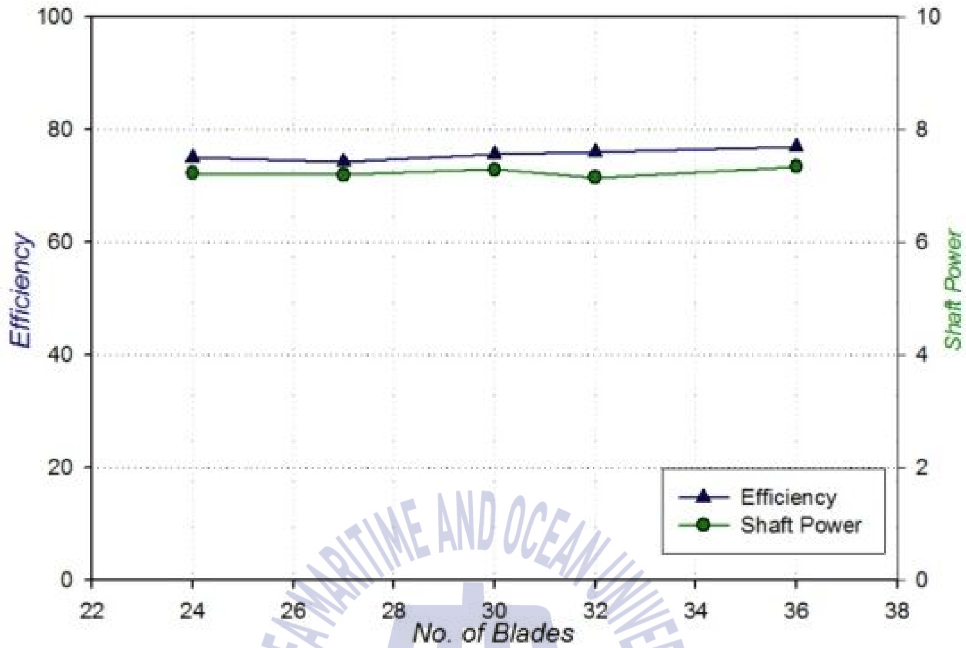

Figure 42 Performance at various numbers of blades at designed condition of 642 rpm and 0.1 m^3/s flow rate

Figure 42 shows the numerical simulation for the different number of blades. As the number of blades increases [15], an increase in efficiency was observed. So a simulation for increased number of blades here shows an increase in efficiency of the turbine. The efficiency for increased number of blades didn't vary much but a slightly increase in blades were observed as the numbers of blades were increased. Efficiency of 76.0% was observed for 32 numbers of blades as compared to 75.6% for 30.

Overall it shows an improvement in the performance of the turbine in changes with the shape of the nozzle, guide vane angle and the number of blades. As the shape of the nozzle has been changed, performance of the turbine can be further improved with the improvement with the change in the shape of the blade angles and ratio. It is seen from the result the changes in shape of the blades according to diameter ratio yield in slightly improved turbine performance and with change in shape of blade inlet angle according to the shape of the nozzle has yield in better performance and efficiency of the turbine can be increased up to 78.90%

4. Static structural analysis

4.1 Static structure

A coupled-field analysis is a multidisciplinary engineering analysis where various independent fields combine and interact together to solve a global engineering problem such that the result of one field is dependent on the other field(s). The coupling can be either one-way or two-way. In the one way coupling, the effect of one field is imposed on the other field but not the vice versa. In the fluid- structure analysis, when the stiffness of the structure is too large, the deflection of such structure has a negligible impact on the flow field. Similarly, in the case of temperature-structure coupling, the temperature field affects the structural field by generating the thermal strains, but the structural strains have a negligible or no impact on the temperature field. For these types of applications, a one-way coupling analysis is sufficient. The classical approach towards one-way FSI is that the pressure distribution on the surface is calculated by CFD, which is exported to FEA to calculate the stresses and deflections on the structure. The effect of the deflection of the structure on the flow field surrounding the structure is neglected in the one-way FSI; hence this type of coupling strategy is also called as a partially-coupled or a weak coupled analysis.

According to the ANSYS coupled-field guide [25], the coupled-field analysis is of two types: Sequential and Direct. The sequential method consists of two or more analyses of different fields, which are executed sequentially. The direct method on the other hand consists of only one analysis in which a coupled field element is used containing information from both the fields. Direct method is mostly used when the coupled-interaction is highly nonlinear.

This thesis only deals with the one way unidirectional FSI. The forces exerted by the water has been extracted into the structural domain and mapped. This has been used to solve the structural analysis

The FSI analysis layout was made in ANSYS workbench as shown in Figure 43. The pressure load from CFX is exported to the structural analysis by defining a Fluid-Structure interface. Also, the boundary conditions of the runner were defined as shown in Figure 45.

The geometries used in the analyses were drawn in the Unigraphics NX 6.0.The FSI analyses were performed by combining CFD analyses in ANSYS CFX and FEM analyses in ANSYS Static structural. The connections between the different programs were done in ANSYS Workbench. Figure 43 shows the workbench connections.

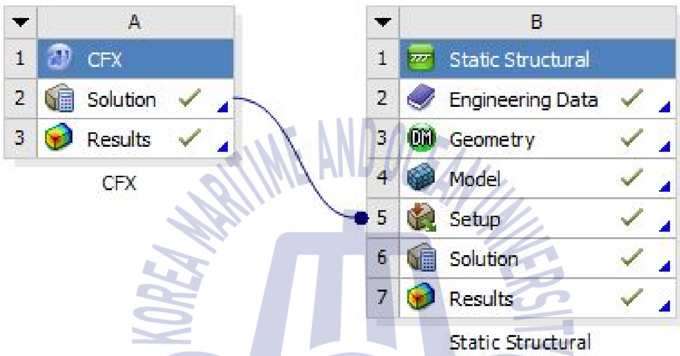

Figure 43 Project schematic of the one-way FSI

4.2 Geometry and meshing

The meshing and structural analysis of the runner was performed in ANSYS Static Structural. A static structural analysis determines the displacement, stresses, strain and forces in structures or components. Figure 44 shows the 3D model of the blade setup where the analysis was conducted. Since the CFD was conducted only for the fluid domain with no intermediate discs, two models: one with intermediate discs and the other without the intermediate discs were constructed to conduct the one way FSI analysis.

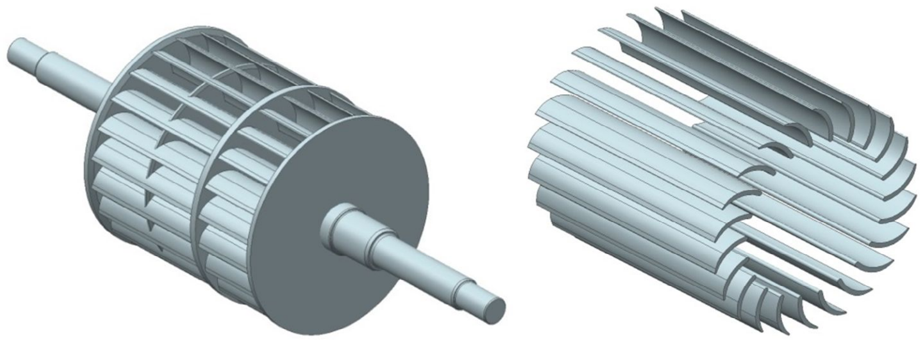

(a) With intermediate discs (b) Without intermediate disc

Figure 44 3D modeling of turbine runner for structural analysis

4.3 Boundary conditions

Figure 45 shows the boundary conditions set in ANSYS mechanical. The boundary condition Fixed support was used on the connecting surface at the sides [26, 27]

- Rotational velocity about the z-axis with 67.23 rad/s.
- Acceleration due to gravity (g).
- Imported pressure load on the blade surface.

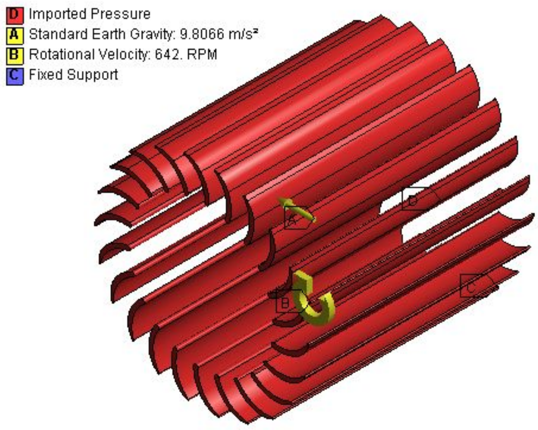

(a) Boundary condition

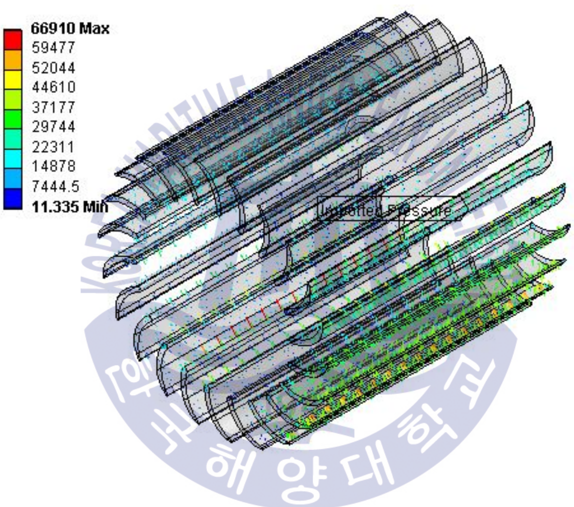

(b) Imported pressure points

Figure 45 Boundary conditions used for the FSI analysis

4.4 Results and analysis

The result of the mesh independent model of Case-I for one-way coupling is shown in Figure 46 and Figure 47. It can be seen that the maximum von-Mises stress is found to be around 32.4 MPa in the reference design and 3.423 MPa in the Turbine case. The position of the maximum von-Mises stress is in the

Pressure side of the blade region connecting the near to the nozzle tip. A comparatively higher amount of stress was found in the second stage of the cross flow runner. Since the water at the stage 1 is at an angle to the runner however at the stage 2 the runner is water hits the regions directly. It can also be seen that due to presence of plates in the middle the stress is evenly distributed in the over the blades in Figure 47 whereas in Figure 46, it can be seen that the stress is mainly concentrated in the middle section of the blade. Considering the experiment was conducted with the other model the stress in the blades is evenly distributed throughout the turbine.

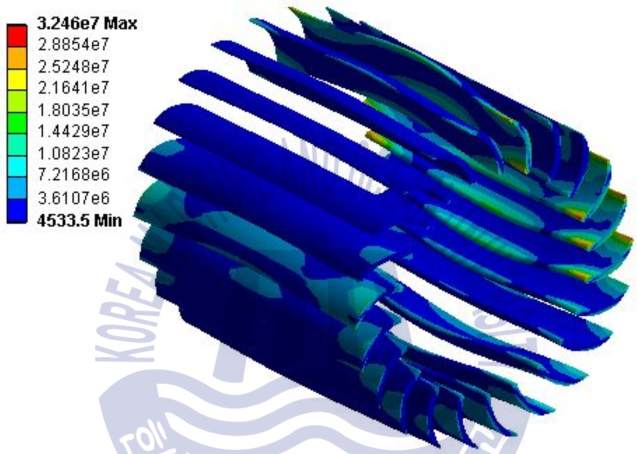

Figure 46 Result of one-way coupling von-Mises stress distribution for turbine without intermediate discs

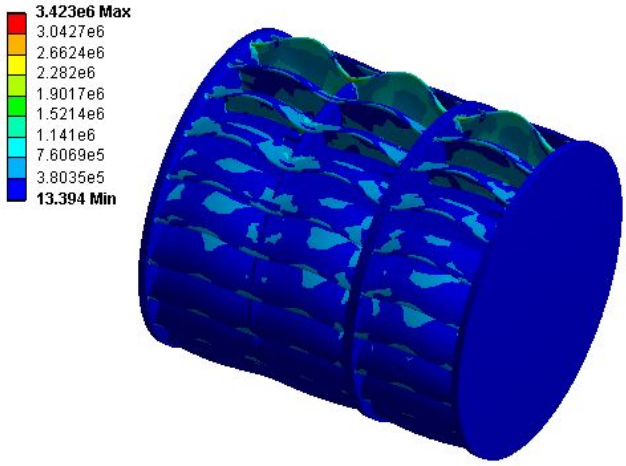

Figure 47 Result of one-way coupling von-Mises stress distribution for turbine with intermediate discs

The deflection in the blades is shown in the Figure 48. The maximum deformation in the turbine blade is for the 2nd stage of the flow. The deflection is mostly around the inlet section of the 2nd stage of cross flow turbine. The total deflection for the blades in the reference turbine was found to be 0.0511mm at the inlet section of 2nd stage transfer whereas for the set up turbine was found to be 0.00124 mm. The maximum deformation is found around the exit for stage 1 and the entry of stage 2. Since the intermediate discs are placed in such turbines, the deformation is distributed throughout the width of the runner.

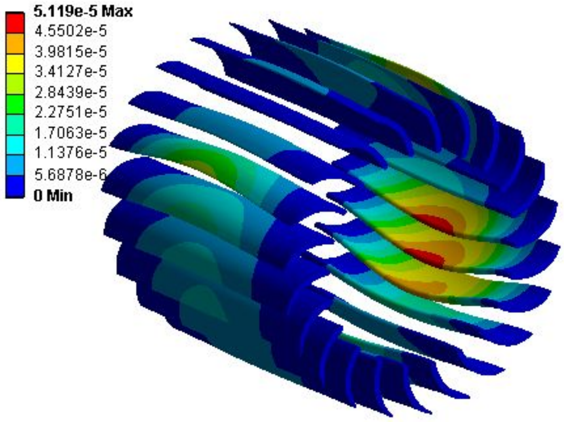

Figure 48 Result of one-way coupling deformation for turbine without intermediate discs

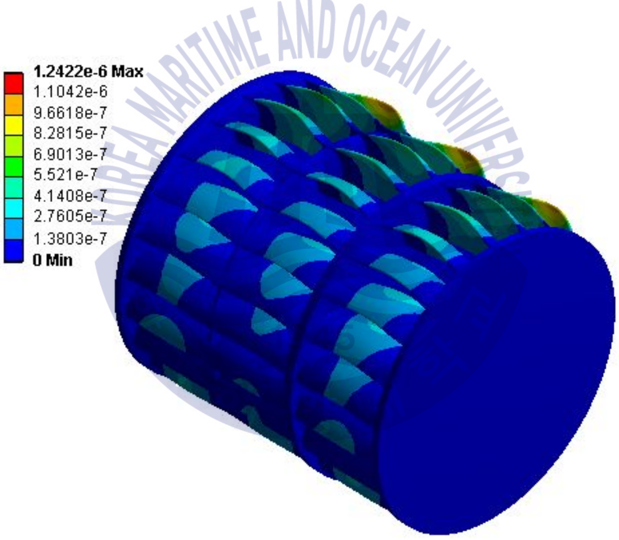

Figure 49 Result of one-way coupling deformation for turbine with intermediate discs

5. Sediment erosion in cross flow turbine

5.1 Sediment erosion

Sediments are the result of fragmentation of rock due to chemical and mechanical weathering. The sediments found in river are mixtures of different particle sizes which cause erosion. Sediment is a naturally occurring material that is broken down by processes of weathering and erosion, and is subsequently transported by the action of wind, water, or ice, and/or by the force of gravity acting on the particle itself.

The mechanism of erosion is much dependent up on the processes, parameters, properties of the impacting particles, target materials and environment. Sediment erosion is a phenomenon of mechanical wear of components, both rotating and stationary, which occurs due to the dynamic action of abrasive sediment flowing in the water impacting against the solid surface of hydraulic components. In case of hydraulic machinery, the suspended sediment in water with kinetic energy, the force of gravity, viscosity, turbulence, centrifuge and cavitation causes mechanical wear.

Table 5 Classification of river sediment [28]

Particle	Clay	Slit	Sand	Gravel	Cobbles	boulders
Size (mm)	< 0.002	0.002-0.06	0.06-2	2-60	60-250	>250

Sediment with specific gravity approximately 2.6 [29] flowing along water passing through the turbine causing the sediment erosion in hydraulic turbine components. Sediment particles are generally divided in to bed load and suspended load based on transport of sediment. If particle move close to the bed by sliding, rolling or jumping, then the particle is called as bed load whereas if particles have much lower velocity than flowing water and are carried away in suspension by flowing water, are called suspended load and they have almost same as the flowing water.

Some of suspended load is settled down in the reservoir or settling basins and rest will strike the turbine resulting erosion. [29]

The intensity of erosion is also directly proportional to the hardness of particles. The particles with hardness value above 5 in Moh's scale are considered harmful. Most of the sediments in Himalayan regions contain more than 70% Quartz particles on average with hardness value of 7 in Mohr's scale, that means sediments are more hazardous to hydraulic components. Based on the wear of base material wear can be classified into abrasive wear and erosive wear.

Abrasive wear occurs every time when a solid material that has equal or greater hardness passes on the particles of a material causing micro cutting, fatigue, grain detachment and brittle fracture resulting the loss of material over a surface. Whereas Erosive wear occurs due to collision of solid and liquid particles on a surface.

Another factor to consider for erosion is the fluid characteristics. Fluid flowing into the turbine possess several characteristics such as velocity, acceleration, impingement angle, medium of flow, temperature, turbulence and many more which is another major aspects contributing to the erosion. The intensity of erosion is directly related to the velocity. Many erosion models have described its relation to the wear is that wear is directly proportional to velocity power '*n*'.

Impingement angle is defined as the angle between the eroded surface and the trajectory of the particle just before impacting a solid surface. If the particles are moving parallel to the surface, impingement angle is almost 0^o and causes only minor. When particles are moving normal to the surface the impingement angle is 90°.Effect of impingement angle is different for different material.

Medium of flow is another aspect to be considered. In case of Hydro power, water is the medium. A mixture of erosive particles and liquid medium is known as slurry. The characteristics of the medium have a strong effect on the final wear rate. Now the controlling factor stands with the medium property such as viscosity, density, turbulence and so on. Many researches indicated that small addition of lubricant to the slurry can notably reduce the erosion.

Material used for the turbine components is the key factor for rate of erosion and their damage. Hardness of the material, its chemical composition, microstructure and its work hardening property determines the intensity of erosion in hydraulic components. The choice of the material for a particular component should be performed according to its ability to meet the functional requirements such as impact strength and ability to withstand the cyclic loading in addition to its wear resistance nature.

Predictions of the erosion in hydraulic turbines are done with the help of various erosion models. These models can help in the design, operation and maintenance of the turbines for a specific site conditions. The erosion models are mostly developed through particle dynamics or empirical and statistical relations obtained from experiments and experiences. The most fundamental form of the erosion model is given by.

Erosion = f (operating condition, properties of the particles, properties of the base material)

The expression for erosion was simplified in [30], which is given in Equation (5-1).

$$\boldsymbol{Erosion \propto (velocity)^m} \qquad \textbf{(5-1)}$$

where m is the exponent of velocity. According to [31], the most general formula for the pure erosion is given by Equation (5-2)

$$W = K_{mat}.K_{env}.C.V_p^m[mm/year] \qquad \textbf{(5-2)}$$

Where W is the erosion rate in mm/year, K_{mat} is the material constant and K_{env} is the environment constant, C is the concentration of the particles and V_p is the velocity of the particle.

An erosion prediction was done based on 8 years of erosion data of 18 hydro-power plants [32] suggested Equation (5-3) to calculate erosion in turbines.

$$W = \beta.C^x.a^y.k_1.k_2.k_3.V^m[mm/year] \qquad \textbf{(5-3)}$$

Where W is loss of thickness per unit time, β is turbine coefficient at eroded part, V is relative flow velocity, a is the average grain size coefficient on the basis of unit value for the grain size 0.05 mm. The terms k_1 and k_2 are shape and hardness coefficient of sand particles and k_3 is the abrasion resistant coefficient of the material. The exponent values x and y are for the concentration and the size coefficient respectively.

According to [33], the erosion rate was estimated through laboratory tests of various turbine materials under different test conditions. Equation 5-4 gives an empirical relation to predict the erosion rate for 16Cr5Ni, which is the most widely, used turbine material.

$$y = 6E - 5 \times 3.13\ [mg/kg] \qquad \textbf{(5-4)}$$

Where x(m/s) is the velocity of eroding particles impinging at the angle of 45° and y is the loss of the material in mg per kg of eroding particles striking the surface.

An erosion model was proposed in [34] that could estimate both absolute erosion rate (mm/year) and corresponding reduction in efficiency (% per year) of Francis runners due to suspended particles. This model was termed as the improved version of the two former models. The final equation yielded by this model was given by Equations (5-5) and (5-6).

$$\boldsymbol{E_r = C.k_{hardness}.k_{shape}.k_m.k_f.a.(size)^b[mm/year]} \quad \textbf{(5-5)}$$

$$\boldsymbol{n_r = a.(E_r)^b[\%/year]} \quad \textbf{(5-6)}$$

Where K_m is the material factor, K_f is the flow factor, K_{shape} is the shape factor and *Khardness* is the hardness factor. *a* and *b* are the empirical constants defined as :

a = 351.35, b = 1.4976 for quartz content of 38%,

a = 1199.8, b = 1.8025 for quartz content of 60%, and

a = 1482.1, b = 1.8125 for quartz content of 80%.

5.2 Basic erosion models in ANSYS-CFX

There are two choices of erosion models in CFX, Finnie and Tabakoff. With a larger number of input parameters, Tabakoff model provides more scope for customization, though the choice between these two models depends on the types of simulation. The equations of these models are discussed below:

5.2.1 Model of Finnie

This model shows that the erosion is affected by the impact angle and the velocity given by a relationship,

$$\boldsymbol{E = kV_p^n f(\gamma)}\textbf{Where,} \quad \textbf{(5-7)}$$

E is a dimensionless mass,

Vp is the particle impact velocity and

$f(\gamma)$ is a dimensionless function of the impact angle which is in radian

n is the value of exponent which is usually in the range of 2.3 to 2.5 for metals.

5.2.2 Model of Tabakoff and Grant

In this model, the erosion rate E is determined from the following relation:

$$\boldsymbol{E = k_1 . f(\gamma) . V_p^2 . cos^2(\gamma)\left[1 - R_T^2\right] + f(V_{PN})} \qquad \textbf{(5-8)}$$

$$\boldsymbol{f(\gamma) = [1 + k_2 . k_{12} . 2\sin(\gamma\frac{\pi/2}{\gamma_0})^2,} \qquad \textbf{(5-9)}$$

$$\boldsymbol{R_T = 1 - k_4 . V_p \sin\gamma,} \qquad \textbf{(5-10)}$$

$$\boldsymbol{f(V_{PN}) = k_3 . (V_p \sin\gamma)^4,} \qquad \textbf{(5-11)}$$

$$\boldsymbol{k_2 = \begin{Bmatrix} 1 \ if \ \gamma \le 2\gamma_0 \\ 0 \ if \ \gamma \ge 2\gamma_0 \end{Bmatrix}} \qquad \textbf{(5-12)}$$

Where,

E is the dimensionless mass (mass of eroded wall material divided by the mass of particle)

V_p is the particle impact velocity

γ is the impact angle in radians between the approaching particle track and the wall

γ_0 is the angle of maximum erosion

k_1 *to* k_4, k_{12} and γ_0 are model constants and depend on the particle/wall material combination.

The Tabakoff model requires the specification of five parameters: The k_{12} constant, 3 reference velocities and the angle of maximum erosion γ. An example of these parameters for Quartz-Steel is shown in Table 6.

Table 6 Coefficients for quartz-steel Tabakoff erosion model

Variable	Coefficient	Value
k_{12}	k_{12}	0.293328
Ref velocity 1	V_1	123.72m/s
Ref Velocity 2	V_2	352.99m/s
Ref Velocity 3	V_3	179.29m/s
Angle of Maximum erosion	$\gamma°$	30°

The erosion rate was predicted for blades of a Cross flow turbines for different shape, size and concentration of the particle and operating conditions of the turbine.

The CFD analysis carried out in ANSYS-CFX contains various parameters shown in Table 7. The generation of the mesh in ICEM CFD, CFX setup and the result showing the erosion rate density for a conventional design is shown in Figure 50.

Table 7 Various CFX parameters used sediment erosion study

Sediment	
Quartz density	2.65 gm/cm3
Particle Molar Mass	1 kg/kmol
Particle Diameter	0.1 mm
Tabakoff erosion parameters	
k_{12}	0.293328
Reference velocity 1	123.72 m/s
Reference velocity 2	352.99 m/s
Reference velocity 3	179.29 m/s
Angle of max. Erosion	30 degree
Particle coupling	One way coupling
Rotating domain	
Angular Velocity	642 rev /min
Turbulence model	SST
R1 Blade/Hub/Shroud boundary detail	No Slip Wall
Inlet components	
Mass flow rate	100 kg/s
Flow direction(cylindrical components)	0 m/s,-1 m/s,0 m/s
Turbulence	Medium (Intensity = 5%)
Particle mass flow rate	0.1 kg/s
Particle position	Uniform injection
Uniform injection	1000 (Direct Specification)
Outlet	
Relative pressure	1 atm
Pres. Profile Blend	0.05
Solver control	
Max. Iterations	500
Residual tolerance	1 E-5

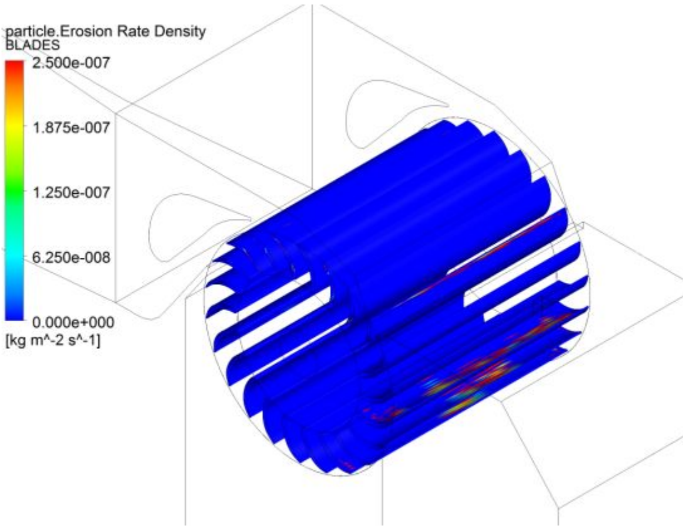

(a) Region of sediment erosion in turbine setup

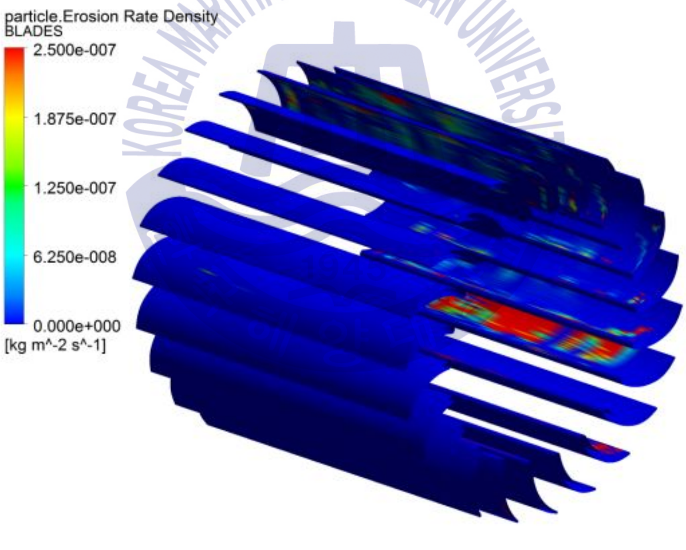

(b) Sediment erosion in turbine runner

Figure 50 Sediment erosions in cross flow turbine

It can be seen form Figure 50, the sediment erosion has mostly influenced in the 2nd stage of the cross flow turbine. During the first phase of the flow, the sediment erosion is less likely but in the second stage it can be seen considerably high. The simulations were done for a single runner passage, where it was shown that the runner at stage 2 of cross flow turbine has the highest effect on the sediment erosion since the runner is in direct contact with the sediment. The particle motion in cross flow turbine shows the particle first hits the pressure side of the stage 1, but the erosion rate density at the pressure stage of stage 1 is not as high in comparison to the erosion rate density at stage 2. The particle motion after it leaves the tip of nozzle shows the sediment under the direct contact with the blades of stage 2 and the region 1 after the nozzle. Since there is no cross flow in region 1, sediment is seen accumulating in that region and the effects of erosion can be highly seen. The sediment erosion rate density is less seen after the water passes through the stage 2. Some traces of sediment were seen in the suction side of the blades in these regions.

5.3 Effect of the size of the particle on the erosion

The intensity of erosion is directly proportional to the size of the particles. Particle sizes above 0.2 mm to 0.25 mm are extremely harmful to turbine components whereas the smaller sized particles wear out the underwater components. The diameter of the quartz particle was chosen to be 0.1 mm for the reference case. The size was now varied between 0.1 mm to 1 mm to observe the effect of the particle diameter on the erosion pattern. Rest of the parameters was made constant.

The results of this analysis are shown in Figure 51 and Figure 52. These figures represent the sediment patterns on the blade on the pressure side, but since all of them have the same 'user specified' range; the comparison of the results cannot be made numerically. Figure 51 represents the average erosion rate density that occurs at the particular size of the particle. The sediment particle size of 0.1 and 0.2 mm diameter area shows minimal effect on the user specified range of sediment erosion whereas the maximum erosion was found around the particle diameter of 0.5 mm. At the diameter 0.4 and 0.5 the sediment erosion is prominent around the blades in stage 2 flow. But with 1 mm diameter the sediment erosion is mostly seen on the first blade at the stage 2 flow and the occurrence is less likely in the other blades, this shows that the size of the particle has a significant but uneven influence on the erosion pattern.

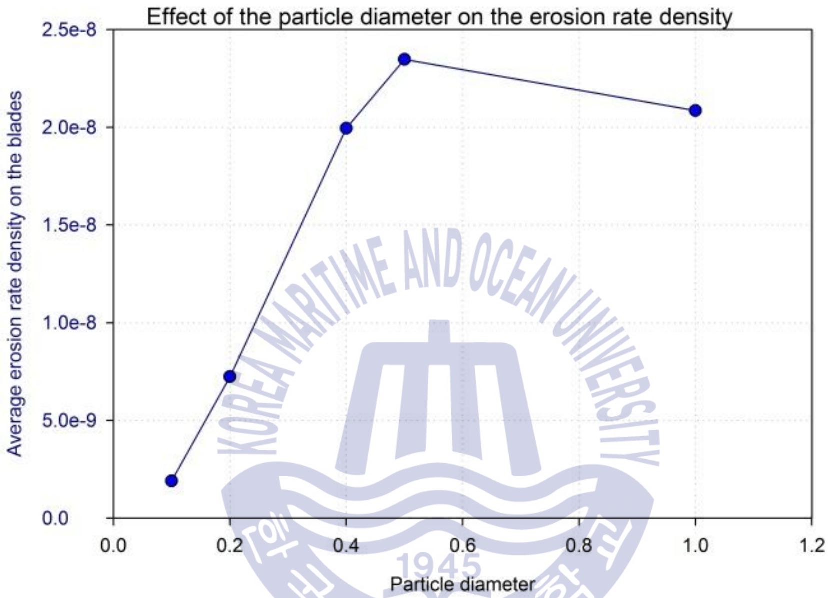

Figure 51 Effect of the sediment size on erosion

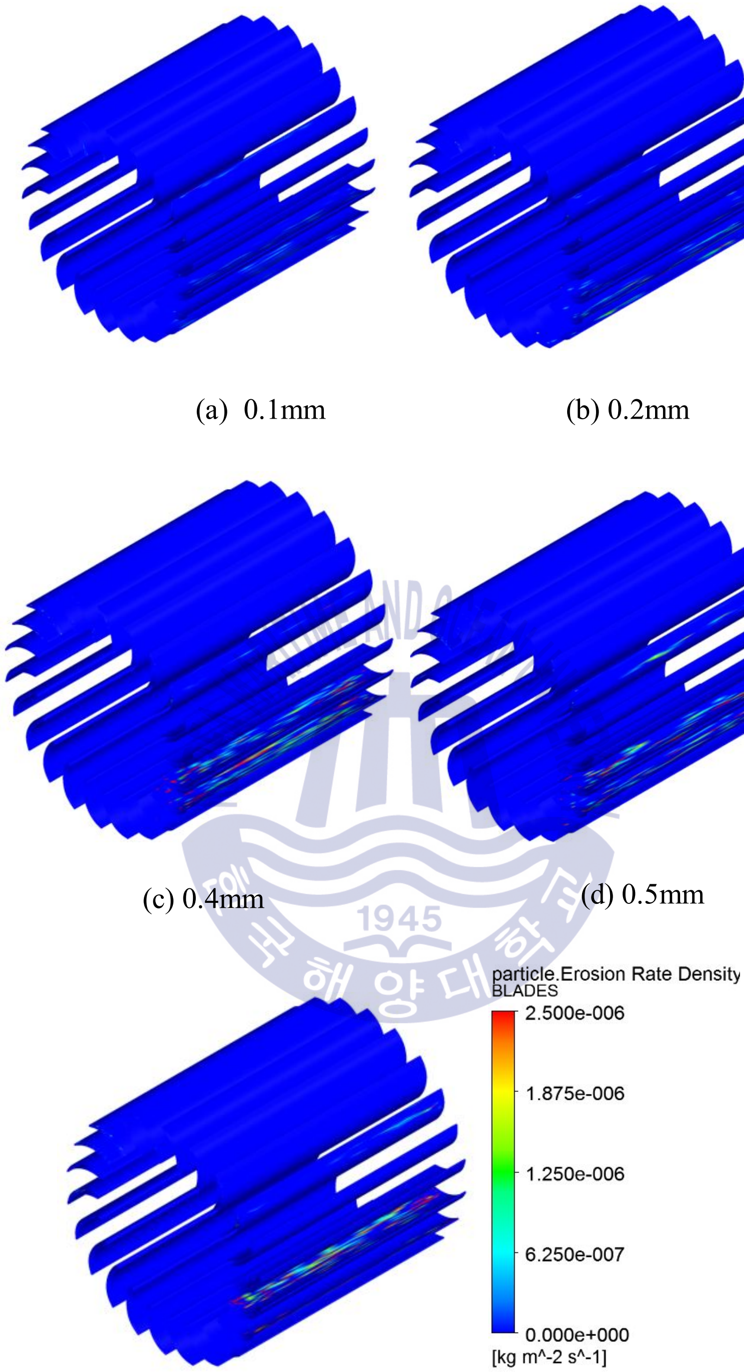

(a) 0.1mm (b) 0.2mm

(c) 0.4mm (d) 0.5mm

(e) 1mm

Figure 52 Effect of sediment size on blades

5.4 Effect of the shape of the particle on the erosion

Generally particle shapes are found round, angular and semi- round based on visual observation experiments using microscope. The shape is defined whether the particles are spherical or elliptical. The X-section area factor of 1 represents the particle of the spherical shape, which was taken in the baseline study. The shape of the particles could however have variable shapes. Here, 2 other shape factors were taken into account. The non-uniformity of the shape was not considered in this study.

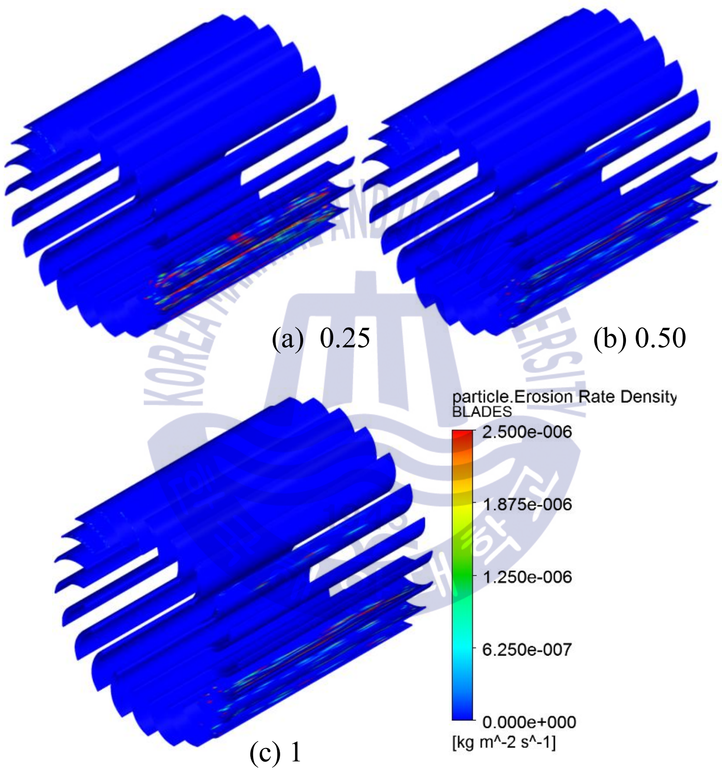

Figure 53 Effect of shape of sediment on blades

Table 8 Average and maximum erosion rate density for different shape sediments

Shape	Average erosion rate density	Max erosion rate density
0.25	2.82892E-08	1.62E-04
0.5	1.64191E-08	1.18E-04
1	6.78416e-009	1.02E-04

The result of this analysis is shown in Figure 53. Erosion rate density is least at shape factor of 1 and increases as value of shape factor decreases. The spherical particle was seen to have the least effect of the erosion compared to the elliptical ones. However, there was not much difference in the overall erosion pattern.

5.5 Effect of the sediment concentration

The sediment concentration is another major dominating factor inducing wear rates. Concentration is termed as the total mass or volume of the particles present in the unit mass or volume of the fluid. Erosion rate is proportional to the concentration of sediment mass up to certain limiting value.

The particles inside the domain can be enabled by defining the 'Particle Behavior' and specifying their properties on the inflow. Here, the particle velocity, injection position, diameter distribution and mass flow rate need to be specified. Here, by default, the injection of the particles is done randomly. The direction of the particle is made identical to the direction of the fluid flow. The particle mass flow rate was varied between 0.01kg/s to 3kg/s per machine. The particle diameter was kept constant (0.1 mm) in this part. The particles are uniformly injected with 1000 number of particles at the inlet. This number can also be chosen as 'Proportional to mass flow rate' where the number of particles per unit mass flow should be specified.

The effect of the mass flow rate of the particle on the average erosion rate density on the blade is shown in Figure 54. It can be seen clearly that the erosion increases linearly with the increase in the mass flow rate. Since other parameters like the injection position, number of particles and the diameter distribution were made constant; the erosion patterns between these mass flow rates were the same. It can be concluded from this analysis that the mass flow rate and the concentration of the uniformly injected sediment particle have a linearly proportional influence on the erosion.

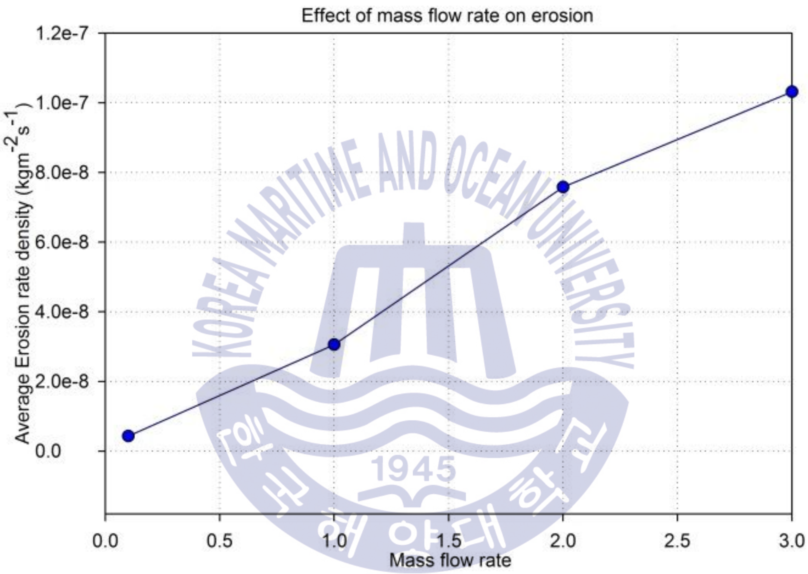

Figure 54 Effect of the mass flow rate on erosion

5.6 Effect of the erosion models on the results

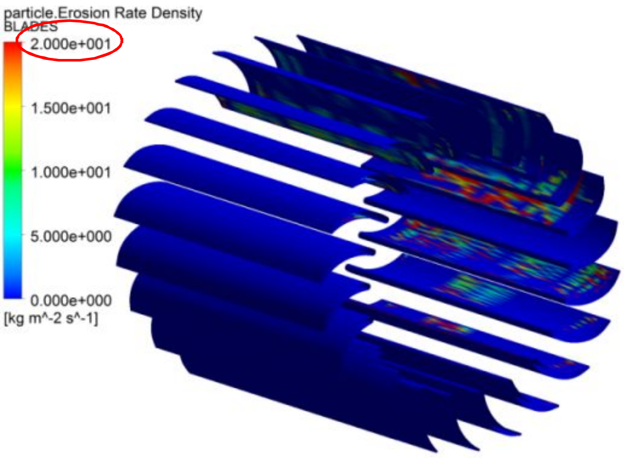

(a) Finnie model

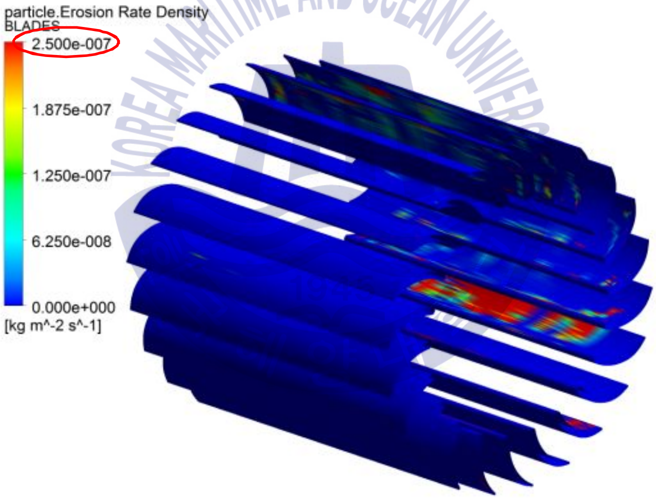

(b) Tabakoff model

Figure 55 Effect of the erosion models

Tabakoff erosion model for Quartz-Steel was used in the baseline study with the values of the parameters provided by ANSYS-CFX. It also supports Finnie erosion model as well as Tabakoff erosion model for Quartz-Steel. These conditions were implemented to observe the variation in the results, which are shown in Figure 55.

In the case of Finnie's model, the erosion is a function of the impact angle and velocity, such that in CFX, the only parameter that could be changed explicitly is the value of the velocity power factor (n) as shown in Equation 5-7. It can be seen from Figure 55 that the amount of erosion predicted by this model is massive even when the value of n is 2 (ranges between 2.3 to 2.5 for metals). This shows that Finnie's erosion model for this case or the parameters provided is not acceptable.

The Tabakoff's erosion model seems to be more promising, especially for this application as the coefficients which are needed for the implementation of the model are already provided by ANSYS-CFX for Quartz-Aluminum and Quartz-Steel. It could be seen from the Figure 55 that when Quartz-Steel is chosen as the eroding and the eroded material. This could be because of the higher density of the steel compared to aluminum. The prediction of the erosion for the stainless steel, which is most commonly used in the hydro turbines, could be more reliable in this case.

6. Conclusions

The processed data from the experiments and the numerical simulation gave valuable information about the cross–flow turbine. The result of the cross flow turbine simulation resulted in the construction of turbine with reduced the number of blades and the modified shape of the nozzle and guide vane angle. The performance study of the designed turbine gave an increase in the efficiency of the turbine up to 69.4% as compared to 61.7% for the previous set up. The shape of the nozzle was changed for the experiment and the guide vane angle for the setup was kept open 7°. The numerical simulation for the same setup gave a turbine efficiency of 71.9%. The values of result obtained from the simulation to the value obtained from the experiment were in close contest.

However the change in the shape of the blade will further improve the efficiency of the turbine. Numerical simulation for the changed shape blade has been conducted. This shows that the change in diameter ratio for the blade can give an efficiency of 75.65% as compared to 73.94% for the designed cross flow turbine. Since the shape of the nozzle has been changed and the shape was blend at the ratio of 150mm, the nozzle exit angle α has been reduced. These changes can be compromised with the change in the shape of the runner inlet. It can be seen that the turbine with low inlet angle gives an increase in efficiency of the turbine. Best efficiency of around 77.5% is obtained for the inlet angle of 20° while keeping the outlet angle constant at 90°.

The FSI analysis of the turbine gives the forces extorted by the water on the turbine. For this study only the forces exerted on the blade has been studied. Pressure points on the blade surfaces has been imported to ANSYS mechanical and mapped at 98% with the structural model. The stress exerted by the water and the deformation of the turbine has been obtained. The study only conducted the one way FSI for the turbine.

The sediment erosion is one of the main researches in the Himalayan Rivers and territory. Since cross flow turbine is easy to manufacture and much simple structure in comparison to other turbines, the sediment research is less focused on it. In this paper, the sediment effect on the turbine has been studied for the various sediment size, shape and sediment mass flow rate. It is seen from the CFD studies that the sediment erosion is mainly occurring in the stage 2 of the turbine. Here the particle is at settling due to gravity and it hits the blade in direct line in comparison to stage 1. The pressure side on the stage 1 and 2 are mostly affected whereas the suction side for the turbines at region 1 and the blade at the tip of the nozzle entry are affected. It is seen that the sediment erosion in turbine increases linearly with the increase in mass flow rate. The more elliptical shape of the sediment is more likely to cause sediment erosion in comparison to spherical shape. The maximum erosion was found for the sediment of around 0.4-0.5mm particle diameter.

Acknowledgements

This thesis has been carried out under the direct supervision of Prof. Lee Young Ho, Division of Mechanical Engineering, Korea Maritime and Ocean University. I am extremely grateful to their constructive advices, suggestions and valuable time that both of them have specified while preparing this thesis. Additionally, my sincere thank is forwarded to colleagues and staffs of PIVLAB for their kind cooperation during the course of this thesis.

I am deeply thankful to the thesis committee, Prof. Park Kweonha (Chairperson, Review Panel) and Prof. Sohn Dongwoo (Co-Chairperson, Review Panel) for their invaluable suggestions and recommendations.

I am extremely thankful to Mr. Nirmal Acharya for providing appropriate information and data during the study. My work would not be completed if I did not get a proper guidance and instructions from PIVLAB students specially Mr. Atmaram Kayastha, Mr. Oblique Shrestha, Mr. Byungha Kim, Mr. Sanyoon Kim, Mr. Jihyun Park Mr. Joji Wata and Mr. Byeongjun Kim.

I would like to thank all my international student friends for their love and support during my stay here in Korea.

Sincere thanks to Prof. Bhola Thapa, Mr. Biraj Singh Thapa and Dr. Hari Prasad Neopane (Kathmandu University) for all their guidance and recommendations for my studies and would like to express my sincere gratitude to Kathmandu University for their kind co-operation and encouragement for the during the course of this thesis.

References

[1] "Annual Report of Nepal Electricity Authority", *NEA, Nepal*, 2015.

[2] "Micro Hydro in Nepal: At a glance", *Jalashakti,* Vol. 3, Nepal, 2014.

[3] Basnet, U., "Renewable Energy Powers Rural Nepal into the Future", *the World Bank*, 2014.

[4] Editorial, *Jalashakti,* Vol. 3, Nepal, 2014.

[5] Energy Forum, "Report of the South Asia Regional Workshop on Developing Standards for Micro- Hydro Sector", Sri Lanka, 2004.

[6] Price, T., Probert, D., "Harnessing Hydropwer: A Practical Guide", *Applied energy,* Vol. 57, No. 2/3, Elsevier Science Ltd., pp. 175-251, 1997.

[7] Kadambi, V., Prasad. K., "An Introduction to Energy conversion", *New age publishers,* Vol. 3, pp. 183, 1977.

[8] Rajput, R.K., Chand, S., "A Textbook of Hydraulic Machinery; Fluid Mechanics and Hydraulic Machines Part-II", 1998.

[9] Tanaka Hydropower co. Ltd., "Turgo Impulse Turbine", Web, 3 April 2015.

[10] Cink-hydro-energy.com, "2-Cell Cross flow Turbine | CINK Hydro-Energy K.S." N.p. Web. 26 Mar. 2015.

[11] "Local Experience with Micro-Hydro Technology", *SKAT*, pp. 171, 1985.

[12] Haimerl, L.A., "The cross-flow turbine", *Water Power Engineering Magazine*, 1960.

[13] Lindsley, E. F., "Water power for your home", *Popular science,* vol. 210, no. 5, pp. 87-93, 1977.

[14] Fiuzat, A. A., Albertson, M. L. and Khosrowpanah, S., "Experimental

study of cross-flow", *Journal of Hydraulic Engineering,* pp. 112 (3), 1988.

[15] Aziz, N. M., and Desai, V. R., "An Experimental Investigation of Cross-Flow Turbine Efficiency", *Journal of Fluid Engineering*, Vol. 116, pp. 545-550, 1994.

[16]Son, S. W. and Choi, Y. D., "Shape Effect of Inlet Nozzle and Draft Tube on the Performance and Internal Flow of Cross- Flow Turbine Hydro Turbine", *Journal of the Korean Society of Marine Engineering*, Vol. 36, No. 3, pp. 351-357, 2012.

[17] Choi, Y. D., Lim, J. I., Kim, Y. T., and Lee, Y. H., "Performance and Internal Flow Characteristics of a Cross- Flow Hydro Turbine by the Shapes of Nozzle and Runner Blade", *Journal of Fluid Science and Technology*, Vol. 3, No. 3, pp. 398-409, 2008.

[18] Olgun, H., "Investigation of the Performance of a Cross- Flow Turbine", *International Journal of Energy Research*, Vol. 22, Issue 11, pp. 953-964, 1998.

[19] Sammartano, V., Aricò, C., Carravetta, A., Fecarotta, O. and Tucciarelli, T., "Banki-Michell Optimal Design by Computational Fluid Dynamics Testing and Hydrodynamic Analysis", *Energies*, Vol. 6, pp. 2362-2385, 2013.

[20] Acharya, N., Kim, C. G., Thapa, B. and Lee, Y. H., "Numerical analysis and performance enhancement of cross-flow turbine", *Journal of Renewable energy*, Vol. 80, pp. 819-826, 2015.

[21] Jesus-De. A., Christian. C., Frank. K., Orlando. A., Auristela. V., and Miguel. A., "Numerical Investigation of the Internal Flow in a Banki Turbine", *International Journal of Rotating Machinery,* Vol. 2011, p. 12, 2010.

[22] Ansys Inc., "ANSYS CFX Reference Guide", Ansys *Inc.*: Canonsburg, PA, USA, 2006.

[23] Ansys Inc., "Two Equation Turbulence Models", ANSYS *CFX- Solver Theory Guide,* 2009.

[24] Mockmore, C. A. and Merryfield, F., "The Banki Water Turbine," *Engineering Experiment Station Bulletin*, No. 25, 1949.

[25] Ansys Inc., "ANSYS Coupled-Field Analysis Guide", *ANSYS Release 10.0*, 2005.

[26] Paulsen, J.B., "FSI-analysis of a Francis turbine", *Master's thesis, NTNU*. 2012,

[27] Chitrakar, S., "FSI Analysis of Francis Turbines Exposed to Sediment Erosion", *Master's Thesis.* 2013.

[28] Lysne. D., Clover. B., Stole. H. and Tesaker. E., "Hydraulic Design", Trondheim: NTNU, 2003.

[29] Neopane. H. P., "Sediment Erosion in Hydro Turbine", *Ph.D. thesis,* NTNU, Trondheim, 2010.

[30] Truscott, G.F., "Literature survey of abrasive wear in hydraulic machinery Wear", pp. 29-50, 1972.

[31] Bardal, E., Korrosjon, Korrosjonsvern, Trondheim: Tapir, 1985 (in Norwegian).

[32] Tsuguo, N., "Estimation of repair cycle of turbine due to abrasion caused by suspended sand and determination of desilting basin capacity", *Proceedings of international seminar on sediment handling technique,* NHA, Kathmandu, 1999.

[33] Thapa, B., "Sand Erosion in Hydraulic Machinery", *PhD thesis,* NTNU, Trondheim, 2004.

[34] Thapa, B.S., Thapa, B., Dahlhaug, O.G., "Empirical modelling of sediment erosion in Francis turbines", *Journal of Energy*, Vol. 41, pp. 386-391, 2012.